

WIRELESSLY POWERED MEDICAL DEVICES: RADIOFREQUENCY TISSUE ABLATION SYSTEM

by

JULIAN MOORE

(Under the Direction of Tsz Ho Tse)

ABSTRACT

In recent decades, wireless power has been used in several industries including medical devices. Radiofrequency tissue ablation is a minimally invasive procedure that treats tumors within the body. In this work, a wireless radiofrequency ablation system was developed and tested. The system is made in two parts – the ablation generator and the wireless catheter. The generator produces a magnetic field that the wireless catheter is placed into and allows an alternating electric current to flow through the tip catheter. Ablation was observed on agar powder ablation phantoms as well as bovine tissue. During testing, a maximum of 15W and 63.27% efficiency was received while the system was able to ablate up to a 2 cm zone. Further improvements can be made to improve efficiency and effectiveness, also modifications can be made to the technology in order to be used in other procedures.

INDEX WORDS: Wireless Power Transfer, Radiofrequency Ablation, Medical Devices

WIRELESSLY POWERED MEDICAL DEVICES: RADIOFREQUENCY TISSUE
ABLATION SYSTEM

by

JULIAN MOORE

BS, University of Georgia, 2017

A Thesis Submitted to the Graduate Faculty of The University of Georgia in Partial Fulfillment
of the Requirements for the Degree

MASTER OF SCIENCE

ATHENS, GEORGIA

2019

© 2019

Julian Moore

All Rights Reserved

WIRELESSLY POWERED MEDICAL DEVICES: RADIOFREQUENCY TISSUE
ABLATION SYSTEM

by

JULIAN MOORE

Major Professor:	Tsz Ho Tse
Committee:	Mable Fok
	Mark Haidekker

Electronic Version Approved:

Suzanne Barbour
Dean of the Graduate School
The University of Georgia
August 2019

TABLE OF CONTENTS

	Page
LIST OF TABLES	vi
LIST OF FIGURES	vii
CHAPTER	
1 Introduction.....	1
2 Applications of Wireless Power Transfer in Medicine: State-of-the-Art Reviews	5
Abstract	6
Introduction.....	6
Methods.....	8
Review Analysis	33
Conclusion	35
Acknowledgements.....	36
3 Modeling Bipolar Radiofrequency Ablation with Thermochromic Agar Phantoms...	37
Introduction.....	37
Methods.....	38
Experimental Results	40
Conclusion	44
4 Developing a Radiofrequency Tumor Ablation System with Wirelessly Powered	
Catheter	46
Introduction.....	46

Methods.....	48
Experimental Results	55
Conclusion	60
Acknowledgements.....	61
5 Battery Powered Wireless Tumor Ablation System and Proposed Future Work.....	62
Introduction.....	62
Methods.....	63
Experimental Results	66
Conclusion and Future Work.....	66
6 Conclusion	68
REFERENCES	71

LIST OF TABLES

	Page
Table 1.1: Engineering Specifications of Current Device and Target Values	4
Table 2.1: Summary of Wireless Power Transfer Medical Implantable Microsystems Reviewed in This Work	32
Table 3.1: Phantom Formula.....	38
Table 4.1: TX Tank Circuit Characteristics	52
Table 4.2: RX Tank Circuit Characteristics.....	53
Table 6.1: Engineering Specifications of Current Device Compared to the Presented System	70

LIST OF FIGURES

	Page
Figure 2.1: The Overview of The Research Process For Each Category	9
Figure 2.2: The left figure shows sketches of the four experimental configurations.	10
Figure 2.3: (a) Expanded view of the magnetic field in tissue multilayers (b) Experimental setup for measuring the transferred power to a moving device, whose properties mimic muscle tissue	11
Figure 2.4: (a) Basic structure of a TET system (b) Overall schematic of the developed TET system	12
Figure 2.5: (a) Schematic of the Implantable Microstimulator (b) In vivo experiment with the LED lighting up at the moment of pulse stimulation.....	13
Figure 2.6: (a) Proposed WPT system (b) Fabricated secondary resonator using a specific geometry (front and back), that maximizes its link efficiency	14
Figure 2.7: (a) Schematic of the H tree distribution (b) Zargham's proposed 3x3cm figure of merit m-sized implant	15
Figure 2.8: (a) From left to right: Primary resonator front and back, Secondary resonator (b) Schematic of the WPT system	17
Figure 2.9: The experimental setup. The transmitting and receiving coils are placed 1 meter apart from another with a relay resonator in between.....	18
Figure 2.10: (a) Microimplant schematic (b) In-vivo system	19

Figure 2.11: (a) Schematic of a segmented coil (b) Front and side view of a wirelessly powered circulatory model	21
Figure 2.12: The left image shows the prototype of the implantable blood flow meter and the right figure shows the orientation of the transmitting and receiving coils.	23
Figure 2.13: (a) An ultrasonic transcutaneous energy transfer system displaying the four energy conversions. (b) Class E amplifier	24
Figure 2.14: (a) Schematic of the wireless powering and monitoring system (b) Implantable ultrasound pulser-receiver prototype	25
Figure 2.15: The design of the capsule robots.	27
Figure 2.16: (a) Left: Three panel view of the cell Right: Actual cell (b) WPT system	28
Figure 2.17: (a) Wireless Powered Capsule Endoscope System (b) Left: Magnetic field generated by a single transmitter. Right: Magnetic field generated by two transmitters.	29
Figure 2.18: (a) Diagram of the Wireless Power Transfer System (b) Experiment Wireless Power Transfer System	31
Figure 3.1: Ablation Setup.....	40
Figure 3.2: The Relationship Between The Amount Of Salt In The Mixture To The Total Phantom Impedance.....	41
Figure 3.3: The Impedance During Ablation at Every Ablation Power.	42
Figure 3.4: The Phantom Temperatures at The Four Probes During Ablation at Each Power.....	44
Figure 4.1: Diagram of the Ablation System.	50
Figure 4.2: Time Domain Analysis of V_{GS} and V_{DS} of the cross coupled MOSFET	51
Figure 4.3: Circuit Diagram of the Transmitting(TX) Circuit.....	52
Figure 4.4: Photo of the (a) TX circuit and (b) TX and RX tank circuit	52

Figure 4.5: Diagram of the Transmitting(TX) and Receiving(RX) Circuits	53
Figure 4.6: The Tip of the Ablation Catheter Prototype	54
Figure 4.7: Diagram of the Receiving(RX) Circuit during testing and ablation	55
Figure 4.8: Diagram of the distance between the TX and RX Coils	55
Figure 4.9: Received power and efficiency as coil distance increases (a) Average received power for 3 trials, Distances at or below 6cm are above the 2.5W ablation minimum, (b) Average received power efficiency at each coil distance for 3 trials	56
Figure 4.10: Received Power and efficiency as DC input voltage increases (a) Average received power for 3 trials, all above the 2.5W ablation minimum, (b) Average received power efficiency for 3 trials, 63.27%	57
Figure 4.11: Setup of the bovine liver experiment (a) ex vivo bovine tissue before ablation, (b) tissue during ablation	58
Figure 4.12: Results of Maximum power test. (a) cross section of ablation zone. 9mm x 18mm, (b) ablation temperatures over time	59
Figure 4.13: Results from the minimum power test. (a) cross section of ablation zone, 12mm x 21mm, (b) ablation temperatures over time	60
Figure 5.1: Transmitting Circuit Diagram	64
Figure 5.2: Ablation generator with all electronics embedded	64
Figure 5.3: The ablation catheter prototype.	65
Figure 5.4: The tip of the ablation catheter prototype	65
Figure 5.5: Results from ex vivo porcine liver test (a) thermal image during ablation, (b) thermal image after ablation (c) image of the 2cm sphere of ablation.....	66

Figure 5.6: Proposed next generation prototype which has an array of transmitting coils embedded into a CT scanning bed.	67
--	----

CHAPTER 1

INTRODUCTION

Wireless power transfer has been increasing in popularity since its invention in the late 19th century. During that time, several principles were introduced including the Ampere-Maxwell Law and Faraday's Law of Induction to calculate the relationship between electrical current and magnetic fields. These theorems provide a detailed explanation on how wireless power works as well as quantifying the size of the magnetic field produced [1].

Due to the rise of small portable devices in recent decades, more batteries have been used to power these devices and the size of the battery is always an engineering limitation. The question of how small the device can be while still being as powerful as possible is the crucial consideration. In addition, the charging cord for these devices can sometimes impede on the portable nature of the device [2, 3].

Many industries have used the theory of wireless power transfer to create effective products that operate smarter and make the easier to use. The electric vehicle industry uses high power wireless power systems to seamlessly charge the battery of an electric vehicle. Another popular wireless power system are wireless mobile phone chargers. These chargers have become common in the past five years where most cell phone manufacturers have receiving coils installed in the newest phone models [4].

In addition to consumer electronics, there are several applications to use wireless power transfer in the medical field. For example, some pacemaker models have batteries that will power

the circuit for a few years. Then, once the battery loses its charge the patient has a surgery to replace the pacemaker battery. Newer and more advanced models of pacemakers use wireless power transfer to charge the battery without the need for an invasive and risky surgery. A full literature review about the applications of wireless power transfer in the medical field is presented in chapter 2 [5]. In this work, 247 published manuscripts were searched through to identify seventeen of the most innovative wireless power systems for the medical field. Those manuscripts were organized into four different categories based on their application: Implants, Pumps, Ultrasound Imaging, and Gastrointestinal Endoscopy. Then, the remainder of this work more specifically focuses on tumor ablation.

Tumor ablation is a minimally invasive method to destroy tumors in the body. Ablation only requires needle sized incisions rather than the larger incisions required for a laparotomy. This procedure is commonly performed on patients who are not good candidates for resection due to their medical history and total risk of the procedure. Ablation systems bring the temperature of the tissue above 60°C which will cause cellular destruction and eventually cell death. There are several different energies used to ablate, however in this work, radiofrequency ablation will be the focus.

Radiofrequency ablation is commonly used to treat lesions in the liver, kidney, lung, bone, breast, prostate and pancreas [6, 7]. This method uses electrical current that alternates at radio frequencies between two electrodes [8-10]. The probe is inserted into the body and contacts the part of tissue the operator wishes to ablate. The tissue introduces a resistance and completes a circuit between the two electrodes. Then when current is applied, the ions in the tissue align in the direction of the current. When that current alternates, the ions agitate, causing tissue coagulation, and thus resulting in cell death [11, 12].

In chapter 3, radiofrequency ablation was observed to understand how heat propagates through tissue. RF ablation phantoms were made from agar power, thermochromic pigment, and a saline solution to quickly ablate a controlled substance. This study compares power, temperature, and impedance against time during the ablation to understand how the ablation zone is formed.

A new radiofrequency ablation device was developed as presented in chapter 4. The ablation system is made in two parts – the ablation generator and the wireless catheter. An amplification circuit was used to amplify the natural oscillations of an LC tank circuit in the proposed generator. The generator produces an alternating magnetic field that the catheter is placed into. Then the wireless catheter is outfitted with a similar LC tank circuit that receives the energy from the magnetic field to power the electric current and ablate tissue. This catheter has the benefit of sterilization because the catheter can be disposable and the catheter can decrease the risk of yanking on the chords that connect the current catheters to the generator.

Engineering Specifications are given that analyze the metrics of a current ablation system. For this example, The AngioDynamics 1500X RF Generator and single probe catheters were used as a base to hypothesis what the target values of the proposed system will be [13, 14].

Finally, in chapter 5, a similar wireless ablation system was proposed. This model is a truly wireless system since the generator is battery powered and free of power cables. The battery powered system is briefly explained and tested to showcase its performance. Then, proposed advancements are provided to show more possible uses of this technology if used in the future.

Engineering Specification		Unit	Current Device Value	Target Value
Catheter	Ablation Tip Length	cm	1-2.5	1 ± 2
	Probe Diameter	gauge	17	17 ± 3
	Thermocouple?	Yes/No	Yes	Yes
	Catheter Wired to Generator?	Yes/No	Yes	No
Generator	Generator Power	W	1-250	1-30
	Generator Frequency	kHz	460	1-500
	Ablation Type	Bi/Mono	Monopolar	Bipolar
	Temperature Control?	Yes/No	Yes	Yes
Results	Maximum Ablation Length	cm	2.75	≥ 2.75
	Maximum Ablation Width	cm	1	≥ 1
	Ablation Time	mins	10	10
	Temperature at Tip	°C	> 60	> 60

Table 1.1. Engineering Specifications of Current Device and Target Values

CHAPTER 2

APPLICATIONS OF WIRELESS POWER TRANSFER IN MEDICINE: STATE-OF-THE-ART REVIEWS¹

¹ Julian Moore, S. Castellanos, S. Xu, B. Wood, H. Ren, and Z.T.H. Tse. *Annals of Biomedical Engineering*. 47.1 (2019): 22-38.

Reprinted here with permission of the publisher.

Abstract

Magnetic resonance within the field of wireless power transfer has seen an increase in popularity over the past decades. This rise can be attributed to the technological advances of electronics and the increased efficiency of popular battery technologies. The same principles of electromagnetic theory can be applied to the medical field. Several medical devices intended for use inside the body use batteries and electrical circuits that could be powered wirelessly. Other medical devices limit the mobility or make patients uncomfortable while in use. The fundamental theory of electromagnetics can improve the field by solving some of these problems. This survey paper summarizes the recent uses and discoveries of wireless power in the medical field. A comprehensive search for papers was conducted using engineering search engines and included papers from related conferences. During the initial search, 247 papers were found then nonrelevant papers were eliminated to leave only suitable material. Seventeen relevant journal papers and/or conference papers were found, then separated into defined categories: Implants, Pumps, Ultrasound Imaging, and Gastrointestinal (GI) Endoscopy. The approach and methods for each paper were analyzed and compared yielding a comprehensive review of these state of the art technologies.

Introduction

Wireless Power Transfer (WPT) exists in several forms, different in terms of used sources, technologies, frequencies and working ranges. Among these, the one using the principles of magnetic induction to deliver power from a transmitting coil to a receiving coil is getting more and more importance. In the majority of cases, a switching electric current is applied to the transmitting coil which produces a magnetic field at a set frequency. When the receiving coil is

placed within the transmitting coil's magnetic field, an electric current is generated in the receiving coil. This switching current can be rectified to produce a DC voltage, which can charge a battery or power a DC circuit [15-17].

The efficiency of the power transfer is directly related to the distance between the coils. The magnetic field becomes exponentially weaker as the distance increases. The most efficient method for WPT, uses the theory of magnetic resonance. In this theory, the resonant frequency is calculated with the total inductance and capacitance of the transmitting coil. When the receiving coil is tuned to the same frequency, the coils will couple and will work at a farther distance [15, 18]. Using these electromagnetic principles to power internal medical devices is appealing to doctors and their patients. In this work, the four types of Medical Implantable Microsystems (MIMs) that will be considered are Implants, Pumps, Ultrasound Imaging, and Gastrointestinal (GI) Endoscopy [19, 20].

Active Implantable Medical Devices (AIMDs) are in vivo devices that aid in or monitor a bodily function. One of the most common AIMDs is the pacemaker, which monitors cardiac rhythms and sends electronic pulses to the heart to correct its rhythm. The primary disadvantage to most AIMDs is their battery life. Invasive surgery could be required to replace the battery. Applying WPT methods prevents the need for surgery and allows the battery to be charged externally [21-24].

Mechanical Pumps within the medical field move fluids or gasses inside the body. A popular medical pump is the Ventricular Assist Device (VAD) which replaces the function of pumping blood in a defective ventricle [25]. A constant supply of power is needed for the VAD so, instead of using an external battery, these pumps can be powered by electromagnetic induction.

A Doppler Flow meter uses ultrasonic imaging to observe the flow of blood through a vascular graft in order to detect a potential failure [26]. These failures are caused by clotting in the graft and require immediate replacement. A single pacemaker battery in an implantable Doppler flow meter system can only last for 5 years. Then surgery is required to replace the battery. Charging the battery or powering the circuit using fundamentals of induction can prevent the need for invasive surgeries.

Endoscopies are the leading standard to observe and diagnose problems in the Gastrointestinal (GI) tract. Commonly conducted with a camera connected to long wire to that enters through the mouth. Endoscopic Capsules are being created and tested to make the procedure faster and painless.

The aim of this manuscript is to identify innovative papers in the area of wirelessly powered medical devices. In the methods section, a brief overview of the selected papers will be provided, then some analysis and suggestions for further work will be given in the proceeding sections.


Methods

The research processes consisted of using the leading scientific research search engines in this field: Google Scholar [27], ScienceDirect [28], IEEE Xplore [29], The IEEE Wireless Power Conference, and The IEEE Transportation Electrification Conference and Expo to find the most relevant articles to the scope of this work. These online databases were used to find relevant articles between 2006 and 2017.

Initially, a general search was conducted with each engine to find any articles related to wireless power in medical devices. Then those articles were processed to eliminate any non-relevant research or duplicate papers across the different search engines. The remaining papers

were scored with a rating scale of 0 (clearly irrelevant) to 10 (clearly relevant). The authors performed a manual scan of each article to assess the scale. The initial search yielded 247 articles, then were filtered to exclude research pertaining to Magnetic Resonance Imaging (MRI) or Ultrasonic Resonance powered devices. Eliminating the non-relevant papers resulted in a total of 17 papers (Fig. 2.1). These papers were separated based on the MIM in reference, Implants, Pumps, Ultrasound Imaging, and Gastrointestinal (GI) Endoscopy. The remaining text in this section will be organized into those four categories.

Initial Article Search				
Implants	Pumps	Ultrasound Imaging	GI Endoscopy	Total
103	36	23	58	247



Exclusion of non-relevant research				
7	3	3	4	17

Figure 2.1. The overview of the research process for each category

Implants

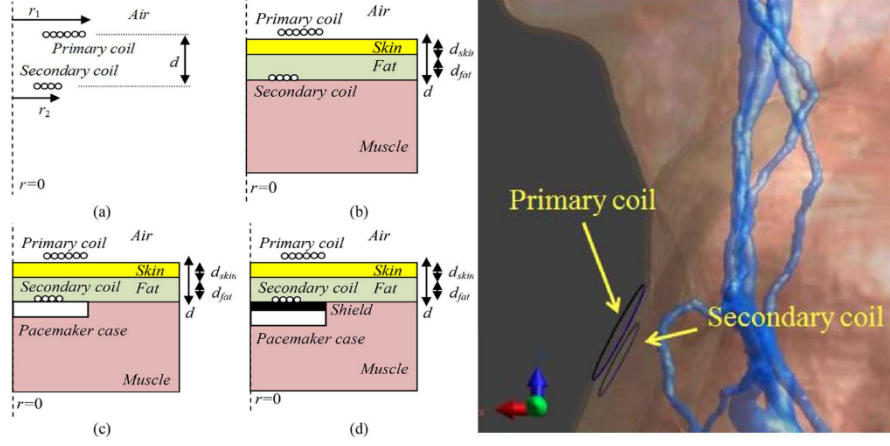


Figure 2.2. The left figure shows sketches of the four experimental configurations. In the first experiment: $d_{skin}=3\text{mm}$, $d_{fat}=2\text{mm}$. In the second experiment, d varied from 10mm to 60mm. The right figure shows the coil positions on an anatomical model.

Campi et al. investigated the safety aspects of wireless power transfer (WPT) to active implantable medical devices (AIMDs) [30]. There are limitations to AIMDs with WPT functionalities because the strong magnetic fields generated pose health risks to humans. However, at certain frequencies, WPT is safe for humans and has many beneficial applications in the medical space.

Experiments were conducted at four different configurations (Fig. 2.2) at both 300kHz and 13.56MHz. The tests observed different capacitor combinations and coil turns to determine each efficiency. In the first configuration, the transmitting and receiving coils are not separated by biological tissues. The second configuration has the receiving coil in biological tissue. The third configuration places the receiving coil in a titanium pacemaker case in the biological tissues, and

the fourth configuration places the receiving coil in the pacemaker case in the tissue, then places a 1mm ferrite shield within the distance.

The first experiment sought to find the efficiencies when the distance between transmitting and receiving coil was set to 5 mm. The results show that the efficiencies at 13.56MHz were greater overall than those at 300kHz. The second experiment determined the efficiencies at each configuration when the distance between coils varied between 10mm to 60mm to account for patients of different sizes. The results from this experiment concluded that the efficiencies rapidly decrease as the distance increases. The series-parallel capacitor configuration at 300kHz and the series-series capacitor configuration at 13.56MHz yielded the most efficient results. Further experiments were conducted to address coil misalignment and impedance-matching, effectively testing the realistic use of WPT to power AIMDs.

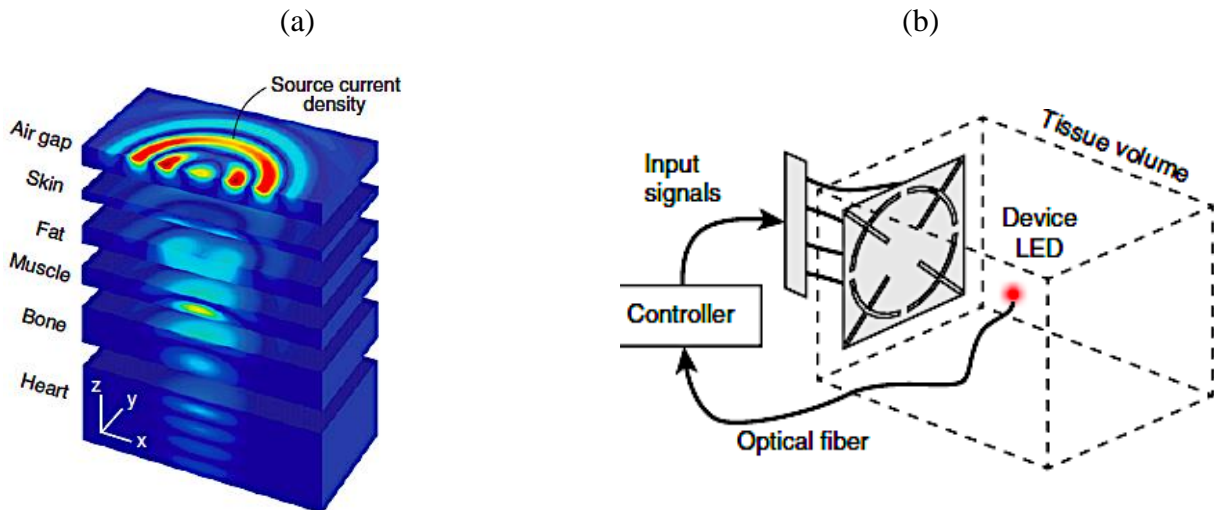


Figure 2.3. (a) Expanded view of the magnetic field in tissue multilayers (b) Experimental setup for measuring the transferred power to a moving device, whose properties mimic muscle tissue.

In this experiment, researchers at Stanford University used a metal plate to control the near field coupling in order to demonstrate milliwatt levels of power transfer to a miniaturized coil in deep heterogeneous tissue [31]. The device consists of a multi-turn coil, rectifier, silicon-on-insulator integrated circuit (IC) for pulse control, and electrodes. Power transfer goes through the multilayer structure, shown in Fig. 2.3a, with the source positioned a subwavelength above the skin layer.

The physical midfield powering source is metal plate patterned with slot-array structures that is excited at four independent radiofrequency ports, then generates circular current paths to determine an approximate current density [32]. Their power transfer device simulations, shown in Fig. 2.3b, are in the left ventricle of the heart and the cortex region of the brain. The measured power transfer to the coil using an initial coupling of 500mW and a separation distance of 5cm, is $195\mu\text{W}$ for the heart and $200\mu\text{W}$ for the brain. When the operating depth is increased to 10cm the received power is about $10\mu\text{W}$. Further tests conducted demonstrated the capabilities of the wireless electro stimulator device by inserting it into the lower epicardium of a rabbit.

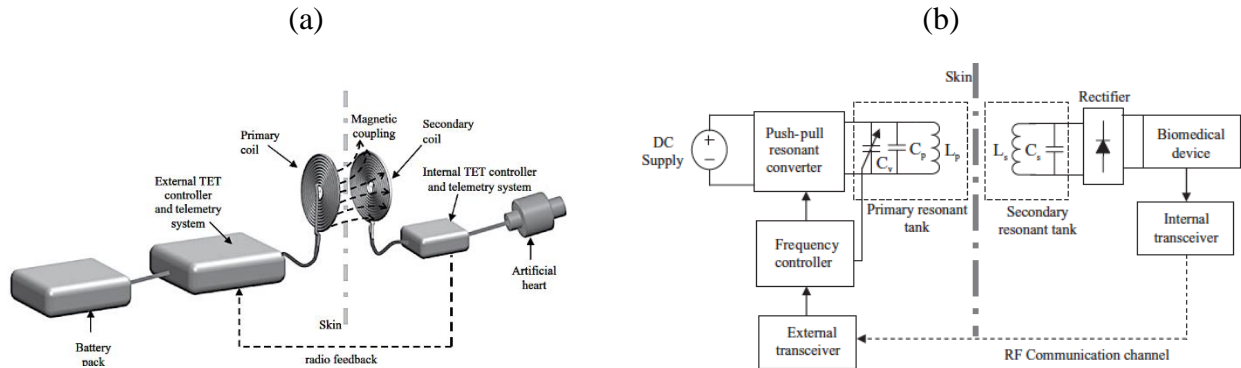


Figure 2.4. (a) Basic structure of a TET system (b) Overall schematic of the developed TET system

Implantable circulatory assist devices require an amount of power that implantable batteries cannot sustain. The current method to receive power is the use of percutaneous leads; however, it can cause infection due to the wires passing through the skin. In transcutaneous energy transfer systems (TET) power is transferred across the skin without direct electrical connectivity using magnetic fields.

In their experiment, researchers at The University of Auckland developed a TET system that uses a closed loop frequency, in the primary power, as a base controller that regulates the power being delivered to a load to compensate for variable coupling conditions [33]. The secondary coil was implanted in six sheep to observe a stable 15 W power output over 4 weeks continuously (Fig.2.4). The experiment's power results ranged from 14.6-15W due to the movement of the sheep which altered the alignment of the primary and secondary coil.

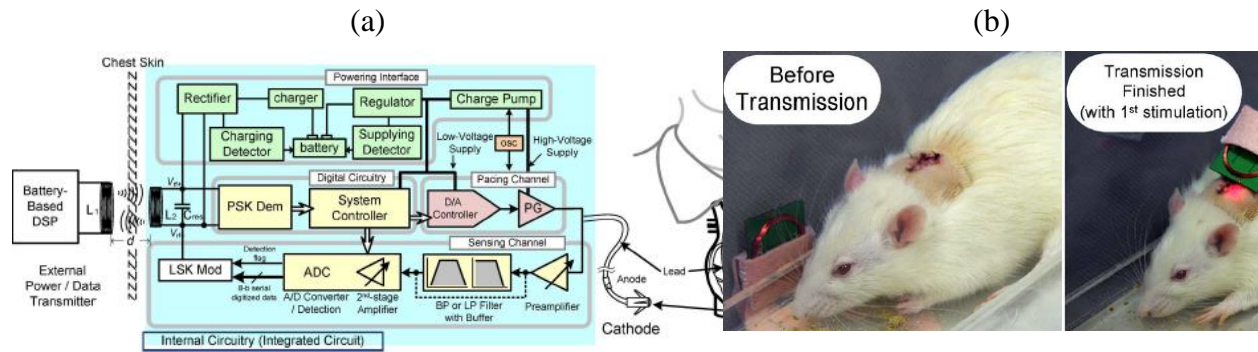


Figure 2.5. (a) Schematic of the Implantable Microstimulator (b) In vivo experiment with the LED lighting up at the moment of pulse stimulation

Lee et. al. developed an external digital signal processor (DSP) that transmits encoded data and charging energy to the internal circuit through a set of coils [34]. The data received is then

transmitted through the body via the same coils. This bidirectional data transmission is achieved using a closed loop implantable microstimulator system on chip (IMSoC). An IMSoC is powered by radio frequency (RF) coupling and is combined with a battery control in order to be utilized as a rechargeable device [35]. The IMSoC, shown in Fig. 2.5a, consists of a power interface that has the ability to control charging, digital circuitry that enhances the reliability in communication, and a pacing channel that has a digital to analog converter (DAC) and a pulse generator. The pacing channel generates stimulation pulses in order to protect the heart from the lack of peak pulses (R-waves).

The in vivo experiment inserts a catheter into the artery toward the right ventricle, an electrode, which coiled in a single loop at the site of cannulation, and the IMSoC. The IMSoC is connected to an external electrode placed in the back of the animal. The operation distance of the IMSoC to the animal is 25-45mm and a R-R beat interval is detected at a rate of 1KHz within a stimulation period of 400ms. The stimulation is visually indicated by the LED shown in Fig. 2.5b.

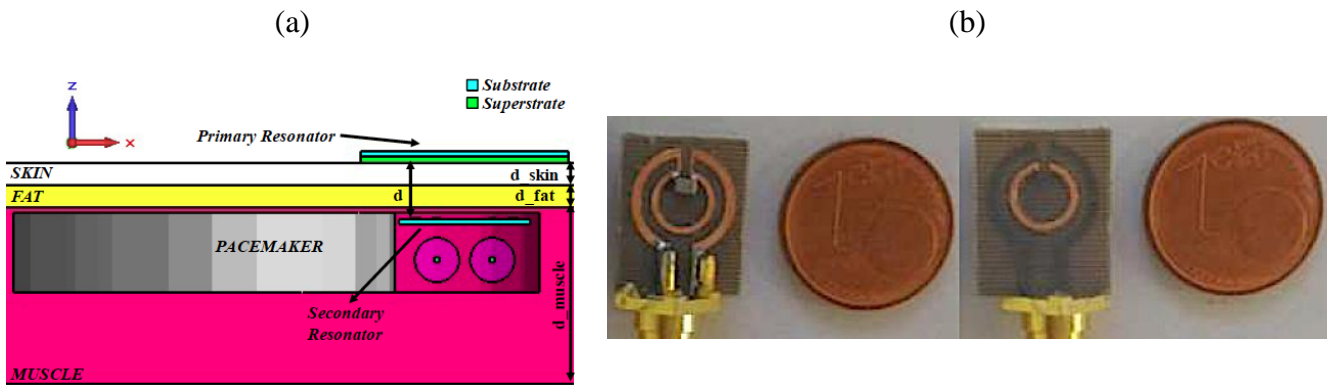


Figure 2.6. (a) Proposed WPT system (b) Fabricated secondary resonator using a specific geometry (front and back), that maximizes its link efficiency

Researchers at the University of Salento developed a wirelessly powered pacemaker [36].

Wireless power transfer for a pacemaker is achieved using RF-to-RF efficiency, shown in Fig.

2.6a. The primary resonator operates outside of the body with direct skin contact and the secondary resonator is integrated in the silicone header of a pacemaker. The resonators undergo a simulation replicating human tissue as well as an experiment using the fabricated resonators, shown in Fig. 2.6b, and minced pork that are connected to a vector network analyzer. The simulator and the ex vivo experiment undergo an impedance load of 50Ω and a frequency of 403MHz in order to produce a 56.8% and 51.4% efficiency, respectively. The system complies with safety regulations by having their specific absorption rate under 2 W/kg per a mass of 10g with a recorded power input of 118mW.

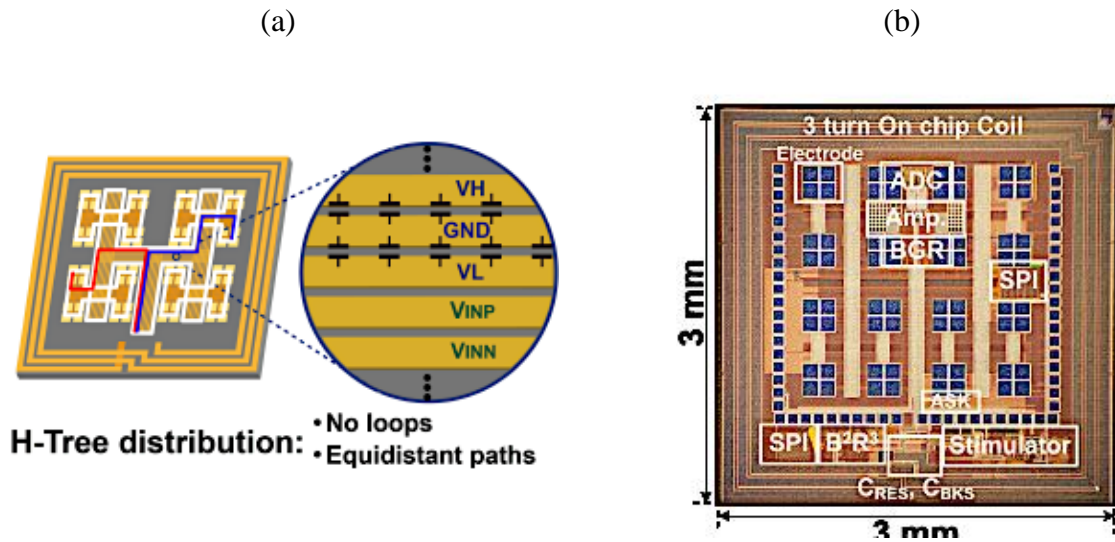


Figure 2.7. (a) Schematic of the H tree distribution (b) Zargham's proposed 3x3cm figure of merit m-sized implant

Kim et. al. developed an ideal wireless power transfer method for miniature implants using electromagnetic waves over ultrasound waves, because the efficiency does not deteriorate with respect to the different acoustic impedances of the tissue layers and the skull [37]. Brain machine interface technologies require miniature implants, to increase longevity, reduce scarring and cell

death, and increase the coverage over the cortical surface [38-42] The power is delivered via a magnetic flux shared by the transmitting and receiving coil, which produces an electromotive force (EMF). The EMF is directly proportional to the area of the receiving coil; thus, the system's efficiency is dependent on the size of the coil. In order to keep the implant small, the operating frequency is increased to an optimal range of 100MHz-1Ghz, which is still under the SAR regulations [43, 44].

The coil's geometry, separation distance, and on-chip design must all maximize the receiving coil's coupling coefficient and minimize its parasitic resistance. A receiving coil with many turns offers a larger voltage and increases the inductance; however, the quality factor of the system can decrease due to a rise in parasitic resistance. The optimal amount of turns for a mm-sized implant is between 2-4 turns at an operating frequency range of 100MHz-300MHz. The receiving coil loses energy and introduces noise due to Eddy currents induced by metal planes or loops. In order to increase the system's efficiency, the on-chip metal loops and planes are removed using an H-tree power network, shown in Fig. 2.7a.

The overall system is also measured by the RF-to-DC conversion efficiency, which is determined by a regulating rectifier's losses. A CMOS fully integrated resonant regulating rectifier uses PWM and PFM in order to activate a conductive path between the resonant tank and the load. Another method is to use an adaptive buck-boost resonant regulating rectifier (B^2R^3). The system uses the boost mode to convert low RF voltage to high regulated DC voltage, and the Buck modes convert large RF voltages down. Figure 2.7b displays a proposed figure of merit of an ideal mm-sized implant that incorporates a 3-turn coil, B^2R^3 , and H-tree power and signal distribution [45].

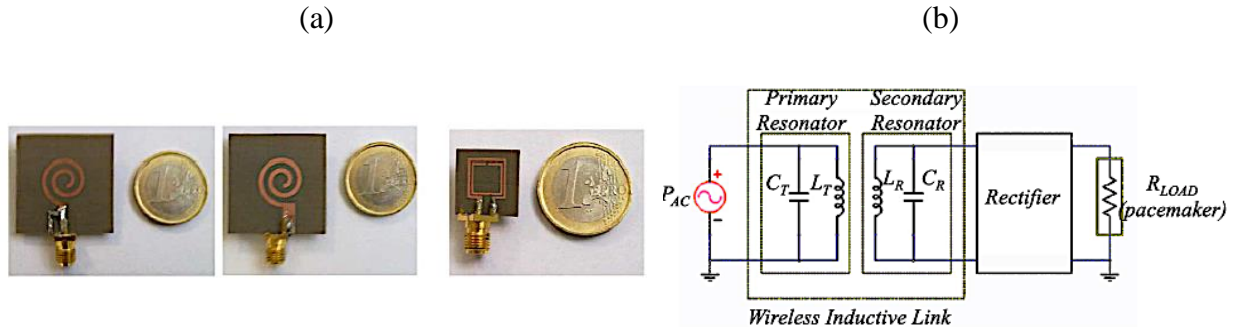


Figure 2.8. (a) From left to right: Primary resonator front and back, Secondary resonator (b) Schematic of the WPT system

Monti et. al. qualified a wireless power transfer technique with the MedRadio band that are intended for implantable medical devices [46]. Operating in the MedRadio Band is reserved for medical devices, allowing it to minimize the interference, and can be used for remote monitoring. The wireless power transfer proposed operates within the MedRadio band, at a frequency of 403MHz, using magnetic coupling. The primary resonator is connected to the power source outside of the body and consists of two planar spirals printed on both sides. This resonator was designed using spiral geometry to optimize parameters using full-wave simulations. The secondary resonator is implanted 5mm under the muscle in order to connect to the medical device, and has a primary loop using a square SSR, shown in Fig. 2.8a [47]. The system experiments using minced pork to replicate the electromagnetic parameters of the homogenous medium from the simulation. It also uses scattering parameters from a vector network analyzer to calculate the power delivered to the implanted device.

The efficiency of the wireless power transfer system, shown in Fig. 2.8b, is sensitive to the resonator distance and misalignment. The efficiency decreased by 3-5% when the receiving resonator was tilted 45° compared to when the resonators are parallel to each other. As the displacement along the x and y axis increases, the efficiency of the system decreases slowly.

Pacemakers have a power consumption range of $10\ \mu\text{W}$ - 1mW . In order to prove this design can produce sufficient power, an AC-to-DC converter is connected to the secondary resonator. The input impedance of the receiver loop and the rectifier is set to 50Ω , since the input impedance of a pacemaker varies significantly, and the resonators were aligned with the primary resonator's distance at 1.5mm from the pork. They varied the power delivered to the primary resonator and measured a value of 60mW , which is sufficient power for a pacemaker. Measurements were also recorded by varying the value of the resistive load in relation to the impedance of the pacemaker, which the maximum load of $330\text{k}\Omega$ resulted in a power output of 1.42mW .

Pumps

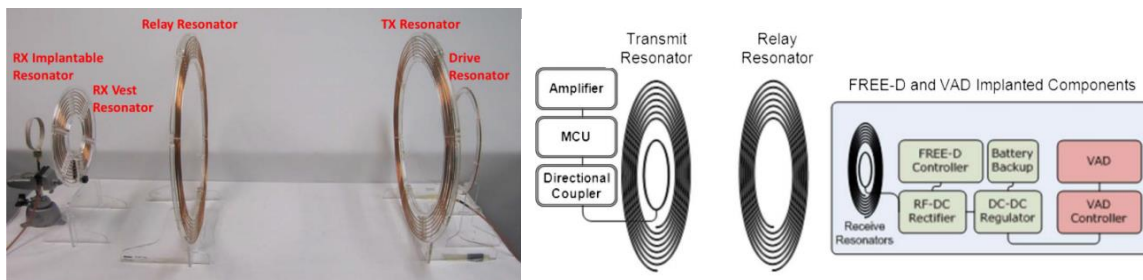


Figure 2.9. The experimental setup. The transmitting and receiving coils are placed 1 meter apart from another with a relay resonator in between.

Waters *et al.* evaluated the use of a Ventricular Assist Device (VAD) with a dynamic Free-Range Resonant Electrical Energy Delivery (FREE-D) System [48]. The intended broader impact for this application is to deliver power to a patient's VAD throughout their homes.

The FREE-D system uses the principles of electromagnetic induction to transfer energy from a transmitting coil to a receiving coil. Two experiments were conducted to test the efficiency

of the FREE-D system when delivering sufficient power to a VAD. The transmitting resonator was placed 1 m away from the receiving resonator with a relay resonator in between (Fig. 2.9).

In the first test, the VAD received a constant 8.1W of rectified power to keep the pump speed at its typical 2400 r/min. The rectified efficiency of the system during this test was 56%, while the resonator efficiency was 85%. In the second test, the pump speed was increased from 1800 r/min to 3000 r/min over two weeks' time, as the VAD power ranged from 4W to 16W. The results showed that as the pump speed increased, so did the amount of power it demanded. The rectified efficiency of the system during this test was approximately 50%, while the resonator efficiency was greater than 90%. No faults or errors occurred during either of the experiments proving the feasibility of using a WPT to power VADs. Further experiments and a more efficient transmission method are needed for successful implementation.

A MATLAB simulation was conducted to demonstrate how efficiencies can increase when using a π -match filter that matches the impedances of the coils to provide maximum power as the distance between the coils change. In the simulation, the impedances in both coils were matched, which increased the efficiency of the system.

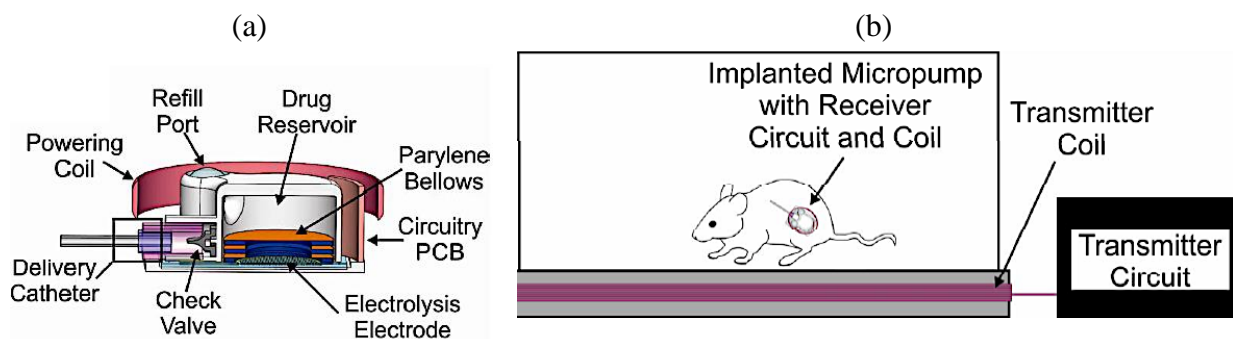


Figure 2.10. (a) Microimplant schematic (b) In-vivo system

Current drug delivery devices for in vivo experiments may cause stress in the animal, which directly impacts the drug's results. Cobo et. al. developed an implantable micropump system to administer the drug on-demand wirelessly [49]. The system, shown in Fig. 2.10a, uses electrolysis, because it has large driving forces, low power consumption, low heat generation, and the ability to control the electronic flow rate.

An external transmitting circuit was created under the animal cage, shown in Fig. 2.10b. It receives an amplified power signal, supplied by a 9V Class E power system, and transmits it to the implanted micropump. The actuator in the implanted device has two electrodes that are in contact with an electrolyte and is separated from the drug reservoir by a polymer bellow. The electrodes cause an increase in pressure of hydrogen and oxygen gas when excited by an electric current. The increase in pressure displaces the fluid and activates the check valve, causing the drug to be administered.

The best results occur when the transmitter and receiver coils are parallel at a stationary state; however, an increase in the coil misalignment and distance causes the flow rate and power transmitted to decrease. The device's flow rate drop range is (42.98% and 64.1%) for a separation distance of 2.5cm and an angle misalignment of 45 degrees. A 30 μ L dosage was administered wirelessly by the micropump with a coil separation of 2cm, and a constant current of .33mA, in order to ensure the device was functioning properly.

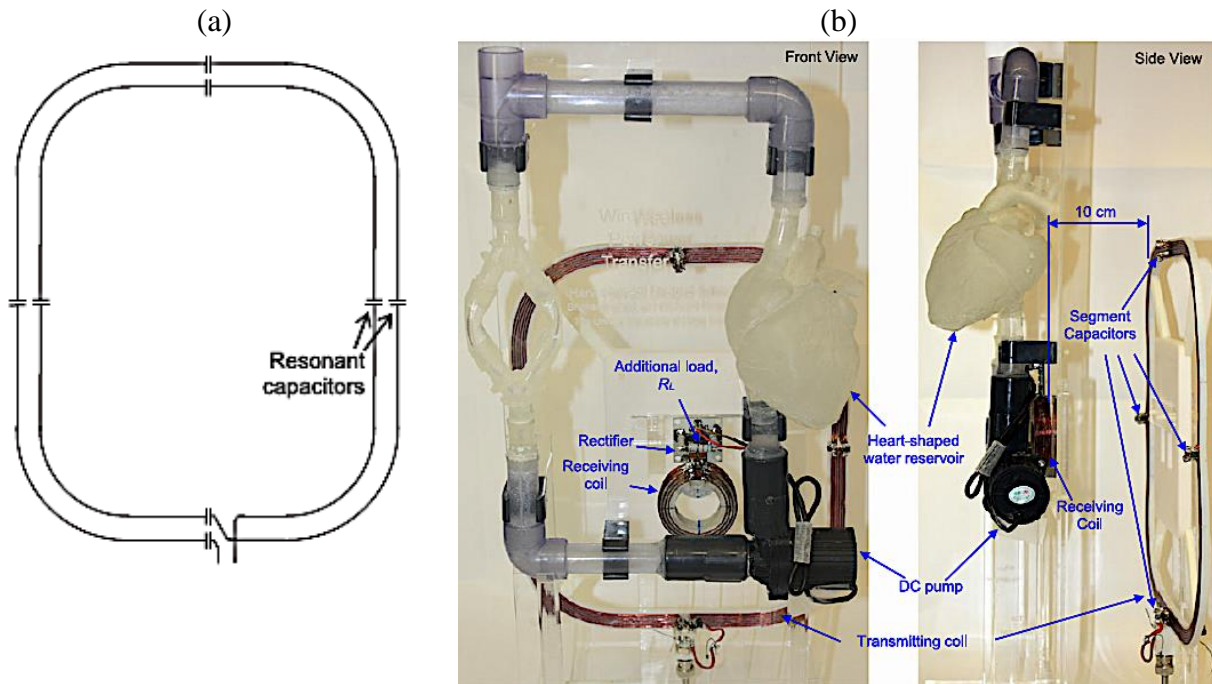


Figure 2.11. (a) Schematic of a segmented coil (b) Front and side view of a wirelessly powered circulatory model

Tang et. al. created a heart pump that was powered by electromagnetic induction so that the pump can be powered from outside the body [50]. Larger transmitting coils in a mid-range wireless power transfer system have the ability to power a deep-seated implantable device without precise coil alignment [51-56]. Mid-range power transfer requires a higher excitation voltage compared to TET systems, thus it consumes more power, is a health risk for the patient, is higher in cost, and the efficiency can change drastically. The mid-range system can have a low operating voltage by dividing the larger transmitting coil into eight segments, shown in Fig. 2.11a, and having a capacitor cancel the voltage across each segment. The magnetic field intensity was analyzed in four large transmitting coils to determine the applicable range. A correlation was observed; by increasing the inner and outer diameter, the energy was able to transfer farther into the body.

In this experiment a rectangular shaped transmitting coil divided into segments is within a vest that the patient wears. The coil does not contain ferrite material causing its inductance of 2.72 μH to remain unaltered in respect to frequency; however, the receiving coil is short and radially thick causing the inductance to become dependent on the location of the coils. The output power and efficiency of the coupling coils remained relatively the same as it was measured under different load conditions and at different separation distances. The maximum efficiency of 80% was recorded when the coils are placed parallel and coaxial with a separation distance of 7.7cm and under a load resistance range of 11-20 Ω . A circulatory model, shown in Fig. 2.11b, was used simulate the flow cycling, and it consists of a DC pump, tubing, and a heart-shaped reservoir. The receiving coil is placed next to a DC pump, which represents a LVAD actuator. The pump is powered via the wireless energy coupling and propels water throughout the system. The power efficiency of the energy coupling coils is 75%, but it is reduced to 54% due to the diode rectifier.

Ultrasound Imaging

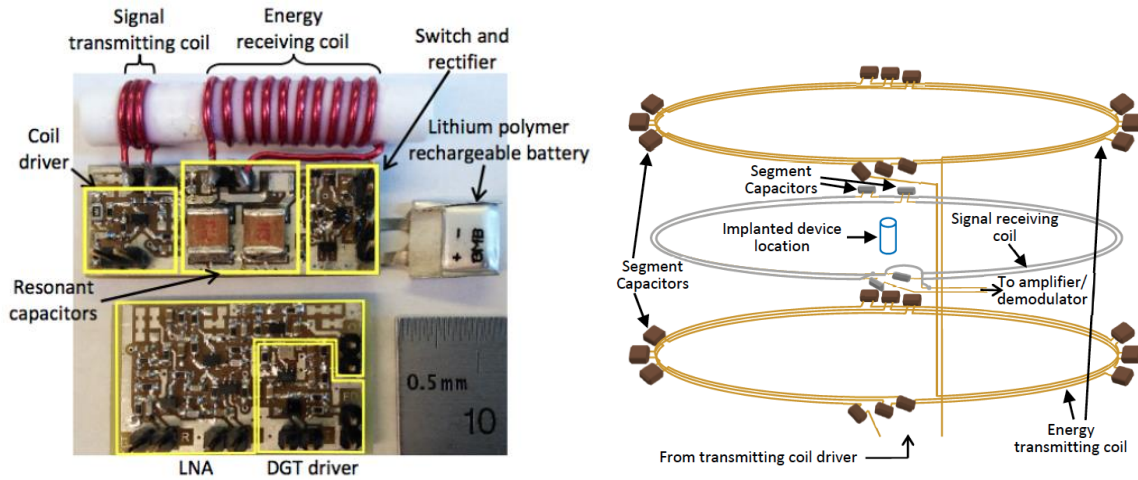


Figure 2.12. The left image shows the prototype of the implantable blood flow meter and the right figure shows the orientation of the transmitting and receiving coils.

Tang et al. aimed to prove the possibility of using magnetic coupling to power an implanted Doppler Flow meter [55]. Using electromagnetic induction to power the implantable system will decrease the cost of the device as well as eliminate the need for various components required for the large internal battery.

A Doppler Flow meter implant prototype (Fig. 2.12) was created on a printed circuit board (PCB), equipped with a power receiver, diffraction-grating transducer (DGT), and a small 8mAh lithium battery. To test the prototype, a fluid with the same conductivity, permittivity, and permeability as human tissue was placed in a cylinder. The meter was connected to the side of the cylinder as the fluid flowed through a graft. The transmitting coil was energized to 2.64 V-rms and 1.6 A-rms at 6.78MHz, while the receiving circuit saw enough power to charge the battery in approximately 20 seconds.

The meter recorded the flow through the graft with a high error due to a low signal-to-noise ratio in the Doppler signal. The system still demonstrates the possibility of wirelessly powering implantable Doppler Flow Meters.

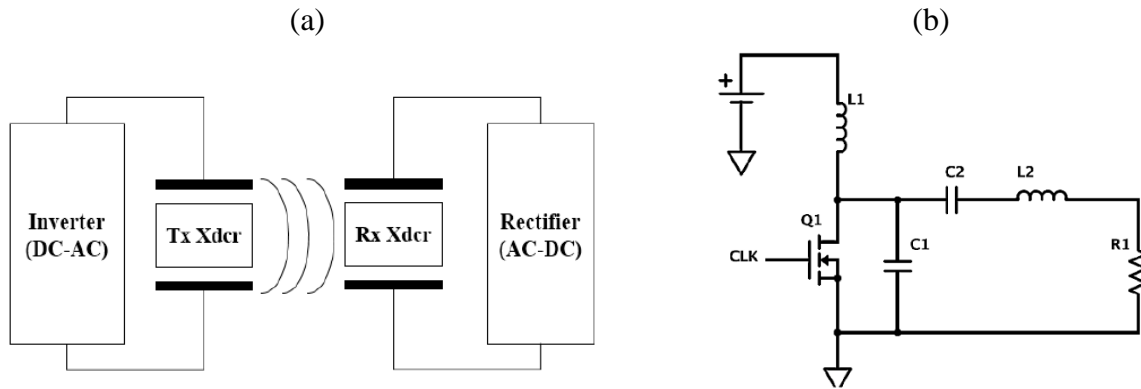


Figure 2.13. (a) An ultrasonic transcutaneous energy transfer system displaying the four energy conversions. (b) Class E amplifier

Vihvelin et. al. developed an ultrasonic power transfer system to power implantable devices [57]. Portable ultrasonic power links require device reliability and maximized battery life, which is achieved by an inverter circuit delivering high efficiency to the transmitting piezoelectric transducer. The efficiency for the wireless ultrasonic power link is the product of each energy conversion shown in Fig. 2.13a. The wireless power transfer process starts when the primary battery sends DC power that is inverted and delivered as AC power to the transmit transducer. The transmit transducer then vibrates and sends a pressure wave that enables the receiving transducer. That transducer converts the pressure waves back into electrical energy. The AC power is converted back into DC via a rectifier.

The inverter is developed in this experiment in order to increase the efficiency of the transmit transducer. Many parameters of the system are defined by the transmitting piezoelectric design requirements such as the input voltage, output voltage, frequency, and output power level.

There are significant source losses that come from the design frequency range derived from the switch-mode amplifier. Another important factor in design of the amplifier is following the ultrasound safety limits, because there is a maximum power level for the transmitter. Therefore, this experiment uses Class E amplifier, shown in Fig. 2.13b, since it minimizes the switches by having the only one at the transistor. In a Class E amplifier, the switch current and voltage waveforms are time-shifted so that the power dissipation is minimized, while the power efficiency is maximized. The amplifier's circuit is simulated using the operating parameters and a range of load impedances. Depending on the frequency it obtained, there was a system loss of 4-9% and a direct correlation such that when the system had a small load, their source loss increased.

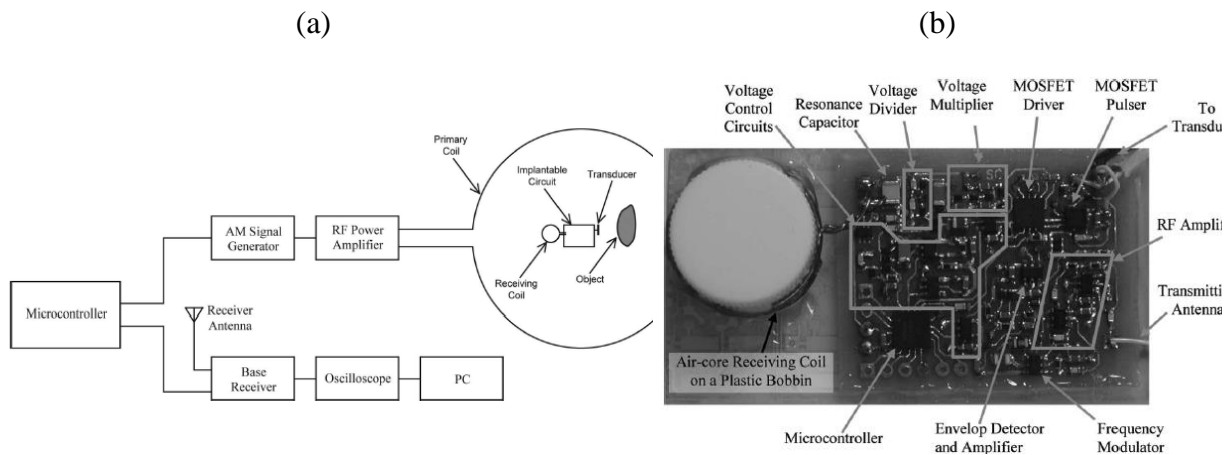


Figure 2.14. (a) Schematic of the wireless powering and monitoring system (b) Implantable ultrasound pulser-receiver prototype

Ultrasonic implantable devices have the potential to monitor deep-seated tissues due to the proximity to air or bone and can monitor organs after transplant surgery [58]. Implantable devices need to have a reliable long-lasting power source. Tang et. al. developed an ultrasonic device (Fig. 2.14a) that is wirelessly powered and monitored externally [53]. Amplitude modulated sinusoidal

currents are generated by a signal generator and amplified in order to excite the primary coil. The system, shown in Fig. 2.14b, has two coils; the primary is wrapped around the body's waist and the secondary coil is deep-seated in the body at the center. Magnetic field coupling is then produced in the primary coil, and it sends the magnetic energy to the secondary coil. The secondary coil then converts the magnetic energy back into electrical energy via electromagnetic induction. The frequency in this design is low in order to prevent magnetic energy absorption in the body. This device sets itself apart from transcutaneous energy systems, because the receiving coil does not contain ferromagnetic material allowing it to be magnetic resonance compatible.

The device begins operation once sufficient power is received by the secondary coil and the induced voltage is then set by capacitor-diode networks. The desired voltage levels supply power to different parts of the device. An ultrasound transducer converts the electrical energy from the pulser to an acoustic wave and vice versa. The acoustic echo signal is transmitted out of the body through an antenna after it is amplified, detected by an envelope, and is carried via frequency-modulate. An external receiver demodulates the FM signal and the waveforms were captured with an oscilloscope.

The prototype was tested at a separation distance of 10cm, and the envelope of the echo signal received by the ultrasound transducer was excited by a 50V pulse. The envelope detected at 172 μ s after the pulse was sent to the transducer, and then the distance between the tank and the wall was calculated using the speed of sound value and the recorded value. They observed that the voltage supply for the pulser is dependent on the secondary's coil position with respect to the center of the primary coil. An ex vivo experiment placed the primary coil around the animal and measured the same envelope signal and DC signal at the moment the pulser was in the air without implantation.

Gastrointestinal (GI) Endoscopy

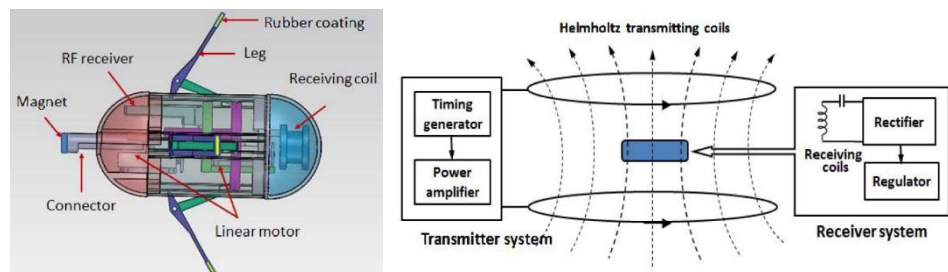


Figure 2.15. The design of the capsule robots. The linear motors are powered electromagnetically by the receiving coil.

Traditional capsule-based endoscopies are relatively small and passively maneuver through the body. This is a non-invasive approach, however there is no control over the direction of the camera or how fast it traverses the GI tract. Several researchers have equipped capsule robots with motors and batteries, in order to have more control over the capsules but are constrained by the size of the capsule. Researchers at The Korea Institute of Technology and Harvard Medical School developed capsule endoscopic robots that work in pairs to perform an endoscopy while powered wirelessly through induction [56].

The capsule system requires a constant 300mW to be powered, thus demanding more power than a battery of an allowable size could supply. Instead of a battery, the capsule robots are equipped with a receiving coil, coupled with the frequency of the transmitting coil, located outside of the body (Fig. 2.15). Their transmitting coil requires a high input voltage up to 32V at 7MHz, in order to safely supply the receiver with at least 300mW at any orientation. Their capsules use a push and pull motion to move through the small intestine. This keeps the capsule stable and allows the operator to adjust the speed and the camera's movement. This prototype proves the feasibility of using WPT to power a capsule based endoscopy, however, the system needs to be miniaturized and further tested.

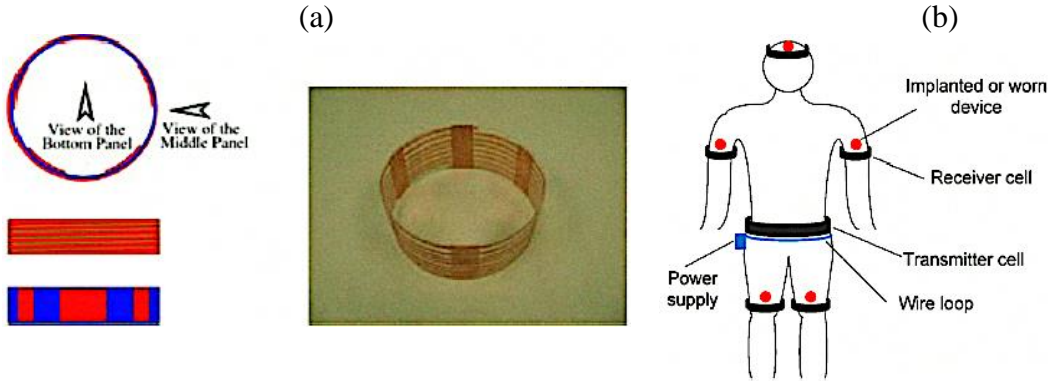


Figure 2.16. (a) Left: Three panel view of the cell Right: Actual cell (b) WPT system

Witricity is a WPT method that uses resonant coupling from thin film resonant cells. Witricity is non-radiative, has a mid-range field, and is designed to be light and flexible [16]. Liu et. al. use the same witricity method and applied it to medical devices inside the body [59]. The thin cell, shown in Fig. 2.16a, has three layers allowing it to create multiple resonant frequencies. Thus, power transmission and data communication can be used simultaneously. The exterior layer acts as an inductor, allowing it to capture and generate the magnetic field. This layer consists of a helical copper tape coil, which creates the ergonomic design of the cell. The middle layer is made of polymer and acts as an insulator by confining most of the electric field. The interior layer contains conductive strips in parallel that form capacitors and divides the inductor.

In their WPT system they use thin film cells as the transmitter and receivers. The system contains one transmitter and multiple receivers, shown in Fig. 2.16b, that are placed on the waist and anywhere near the implanted/worn devices, respectively. The transmitter is coupled with a power driving loop and the load's driving circuit is inductively coupled with a receiver. The coupling of the receiver is achieved with a single coil and multiple turns. The voltage and power are directly associated with the number of turns.

This experiment lacked accuracy because they used convenient measurements for the load, which directly affected the measured voltage and the calculated power values. The article does not

provide values for their voltage and power; however, their experiment yielded a 40% efficiency at a distance of 20cm. The other applications in Table 1. have higher efficiencies and larger frequencies. The insulation layer of the thin cell should be researched in this WPT system, since it has lower frequencies that are beneficial.

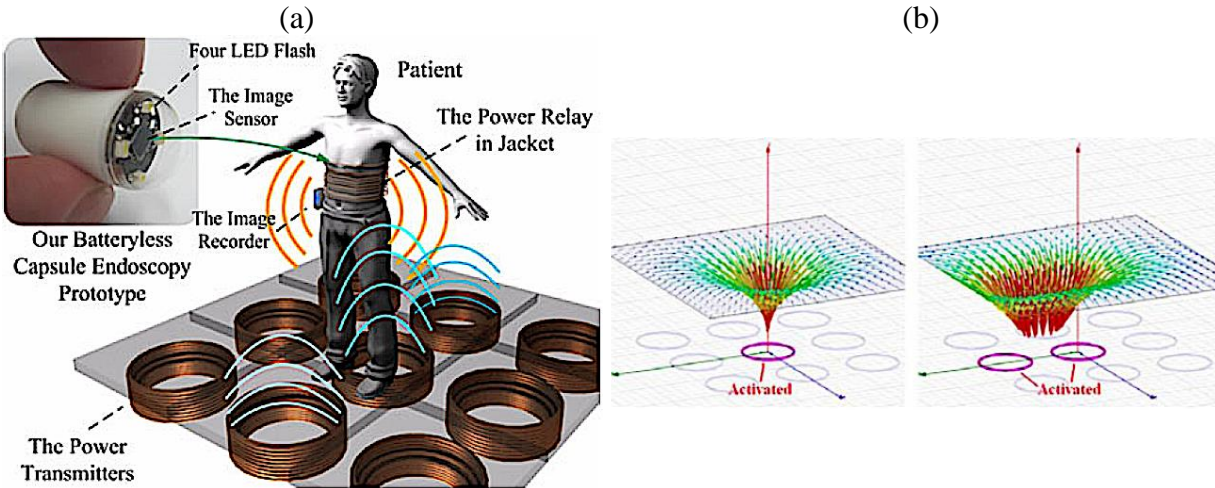


Figure 2.17. (a) Wireless Powered Capsule Endoscopy System (b) Left: Magnetic field generated by a single transmitter. Right: Magnetic field generated by two transmitters.

Wireless capsule endoscopes (WCE) require patients to wear a jacket with antennas and a power transmitter that is connected to an external power source via a long power cable [60, 61]. The patient's mobility is restricted making it uncomfortable for them both psychologically and physically. Sun et. al. proposed a WCE system (Fig. 2.17a) to increase mobility using a wireless power transmitter array installed under the floor [62]. This allows the patient to wear a jacket that has a resonant antenna and still be able to move around the room unrestricted. Pressure sensors are able to identify the position of the patient by activating the nearest transmitter to generate wireless power. The power is delivered to the jacket and the capsule inside the patient picks up energy from the power relay. The distance of the system is 5-30 times greater than other current WCE systems [63, 64].

The floor consists of pressure sensors that determine the patient's position, shown in Fig. 2.17b, and only one transmitter is activated at a time. When a patient is walking between two transmitters, the first transmitter is turned off once the second transmitter is turned on by a switching operation. There are nine transmitters in an array, and stability is ensured by using the strong-coupling technique and Schmitt triggers for all the switches.

In this WPT system the first hop consists of a strong-coupling mechanism with high resonators, while the second hop has loose coupling with small antennas. The dropout voltage and switch timing of rectifiers can determine the efficiency in the wirelessly powered implant [65-69]. The experiment shows that the patient's lateral alignments determine the transfer efficiency. When the patient is directly above the transmitter and the capsule is positioned near the power relay, the efficiency is at its peak. The reason for the shift in efficiency is the loose coupling in the two-hop step.

Ingestible wireless capsules have restricted locomotion, battery power, ability to stop, and can only be used for one organ. However, wireless capsule endoscopy (WCE) is a solution that can be tolerated by the patients, does not require sedation, and does not entail radiation absorption. WCE can also be used on patients that have portable electric cardiac devices [70]. The first ingestible capsule is the M2A, which has the capability to take more than 55 thousand 140° images during the eight-hour process, and also have its position located. The M2A sent images via radiofrequency to an antenna array that is taped to the abdomen, and its position was determined by a triangulation process of the signal strength received [71, 72]. The EndoCapsule was developed after as a self-disintegrating pill that is located by radiofrequency and has a sensor camera allowing physicians to view real-time images [73]. The SmartPill is another advanced WCE containing three sensors to monitor the pH, temperature, and pressure inside the GI tract.

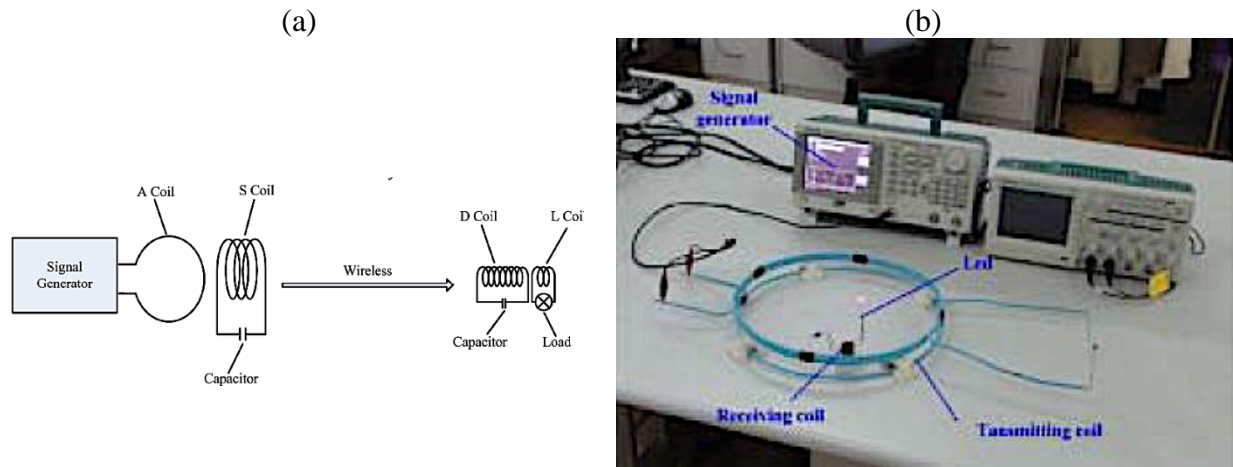


Figure 2.18. (a) Diagram of the Wireless Power Transfer System (b) Experiment WPT system

Fang et. al. developed another wireless capsule endoscope system that uses electromagnetic induction [63]. To implement this in capsule endoscopy, the size of the receiving coils must be limited, while maintaining a high system efficiency. The WPT system, shown in Fig. 2.18a, has two large coils for energy emission and two small coils for energy receiving. The coil parameters influence the frequency, and the quality factor affects the power loss of coils. For this experiment, they used silver-plated copper wire to increase the surface conductivity of the conductor and prevent additional dielectric loss. The quality factor of coil is improved by the number of turns and radius of the coil; however, the capsule endoscopy limits the experiment to hollow single coils.

The experiment system, shown in Fig. 2.18b, is comprised of two coils as the receiver, a signal generator for the transmitter, and a light-emitting diode as the final load. The purpose of this experiment was to measure the transmission and received power using an oscilloscope in order to calculate the efficiency. The results yielded a correlation between the efficiency of the system and the distance between the transmission coils. The best performance of the system is when the transmission coil distance is at the focal length.

TABLE 1: SUMMARY OF WIRELESS POWER TRANSFER MEDICAL IMPLANTABLE MICROSYSTEMS REVIEWED IN THIS WORK

APPLICATION		Frequency	Transmitting Voltage	Receiving Power	Distance	Receiving Coil Size	Transmitting Coil Size	Efficiency	Topology
IMPLANTS	CHARGING AIMDS AND PACEMAKERS[30]	300kHz, 13.56MHz	0.2-5.15V	1 W	5mm, 10-60mm	17.65 mm	18.3 mm	Varies, up to 95%	Circular planar coils, 1-10 turns
	DEEP-TISSUE MICROIMPLANTS[31]	1.6 GHz	2V	1.7-2.2mW	5.5cm	2mm diameter	N/A	N/A	Multi-turn 1-15 turns
	TRANSCUTANEOUS ENERGY TRANSFER IMPLANT[33]	156.5-185.4KHz	12V	15W	10-20mm	50mm diameter	50mm diameter	Varies, up to 80%	2 coils
	ENDOCARDIAL STIMULATION FOR CARDIAC PACEMAKER[34]	256kHz	1V	48μW	25-45 mm	~1.5 x 1.6 mm ²	N/A	N/A	Small multi-turn coils
	RECHARGEABLE PACEMAKERS[36]	403 MHz	N/A	110 mW - 118 mW	5 mm	~4.94 mm	~ 7.53 mm	~ 51%	PCB spiral
	MINIATURIZED IMPLANTS[37]	Up to 100MHz	4.5V	Up to 100μW	5-15 mm	1-8 mm	N/A	68%	Three-turn on-chip Rx
	REMOTE POWERING OF PACEMAKERS[46]	403MHz	N/A	80 mW	5 mm	9.5 x 9.5 mm ²	9.5 x 9.5 mm ²	5.24%	PCB coils
PUMPS	POWERING VENTRICLE ASSIST DEVICES[48]	13.56MHz	N/A	4-16W	1m	9.3 cm	9.3 cm	> 85%, rectified: 45% to 50%	PCB coils
	INFUSION MICROPUMP[49]	2MHz	9V	N/A	2-4cm	17mm diameter	310x140mm	N/A	Transmitter: 8 turns Receiver: 6 turns
	IMPLANTABLE HEART PUMP[50]	6.78MHz	8.57Vrms	19.7W	10cm	5.3cm diameter, 1.24cm height	1.2mm diameter	54%	Transmitter: 2 turns Receiver: 1 turn, 4 layers
ULTRASOUND IMAGING	DOPPLER SYSTEM FOR VASCULAR GRAFTS[55]	6.78MHz	2.64 V-rms	60mA	~10cm	20 cm diameter, 10 turns	N/A	N/A	Helmholtz configuration
	CLASS E RF AMPLIFIER IN ULTRASONIC LINKS[57]	1.275 MHz	3.3V or 5V	293mW	N/A	N/A	N/A	90%	N/A
	DEEP-SEAED IMPANTABLE ULTRASONIC PULSER-RECIEVER[58]	5.7 MHz	12.5-50V	12mW	14cm	2cm diameter	30cm diameter	N/A	Primary coil- 1 turn Secondary coil-5 turns

GASTROINTESTINAL (GI) ENDOSCOPY	MODULAR CAPUSLE ENDOSCOPES[56]	7 MHz	32V	300-700mW	> 50m	2cm diameter, 1cm height	N/A	varies	Helmholtz transmitting coils, Rx: 14 turns
	WITRICITY[59]	7.02-7.04 MHz	N/A	N/A	10 cm	16.26cm diameter, 6.71cm height	35.2 cm diameter, 29mm height	Varies, up to 75%	2 coils Transmitter: 4 turns Receiver: 7 turns
	TWO-HOP WIRELESS CAPSULE ENDOSCOPY[62]	13.56 MHz	0-10V	24-90 mW	1m	11mm diameter	48cm diameter	Varies, up to 39.8%	First hop: 4 coils Second hop: 2 coils
	MAGNETIC RESONANCE WCE[63]	8.2MHz	N/A	Varies, up to 51.6mW	Varies, up to 4cm	.6cm diameter	15cm diameter	Varies, up to 26.14%	4 coils Turns A coil:1 S coil:3 D coil:10 L coil: 3

Review Analysis

From the initial article search, 17 were found to be relevant research to the scope of this work. Most of the non-relevant material focused on the applications of the specific technology and did not introduce a new medical device hardware that incorporated the use of electromagnetic wireless power transfer. The selected papers all aimed to improve the field of medical implantable microsystems with electromagnetic wireless power transfer. The majority of the relevant papers were classified as implant-related where the ultrasound imaging and pump categories contained the least amount of papers. Table 1 consolidates the methods from each paper reviewed and allows easy comparison between different technologies and applications. A summary of future challenges and hurdles to implementation are presented below.

Future Work

Due to the recent introduction of these devices, most of the devices were in the early prototype phase and intended to prove their concept before the researchers move on to clinical testing. Further work is needed to increase the efficiency of the wireless power transmission.

Many of the reviewed articles contained prototypes with size limitations. The coil geometry constrained the overall size of the prototypes. The relationship between the diameter of the receiving and transmitting coils must be maintained to ensure an efficient transfer of energy. The motor size for some of the endoscopes reviewed also contributed to the size limitation. These researchers need to either re-arrange the components in their prototype or find smaller motors that will work in their design. Other potential risks are centered around heating. The electronics both on the transmitting and receiving side can produce high levels of heat that can be harmful for patients or equipment operators. Special measures should be taken in order to dissipate the heat in a safe way for the people involved.

Regulation

In order for these state of the art technologies to be adopted and used on human patients, they must be approved by clinical regulatory agencies. The U.S. Food and Drug Administration (FDA) and European Medicines Agency (EMA) are two organizations in place to ensure the reliability, user safety, and ease of use for new medical technologies. The technologies reviewed in this paper can be adopted to medical practice only when they follow regulations and improve the medical field.

Lack of clinical trials can be partially attributed to the safety risk WPT poses. WPT can induce heating caused by radio frequency (RF) absorption in the body. Therefore, the maximum specific absorption rate (SAR) is set to be 2W/kg per 10g human body according to the International Commission on Non-Ionizing Radiation Protection (ICNIRP) regulation [74]. There are certain transmitting frequencies that are prohibited by most countries. These frequencies are either unsafe for human interaction or they pose electromagnetic compatibility (EMC) risks [75].

Funding

The field of wireless medical devices have been receiving attention because of its potential to shape the future of the medical field. The total amount of money awarded to those researching wireless medical devices has been on the rise. Figure 19 shows the total award amount from the National Science Foundation (NSF) and National Institutes of Health (NIH) per year for grants involving wireless medical devices [76]. The funding for this field is steadily increasing and progress is assumed to continue.

Conclusion

Wireless Power Transfer has several possible applications within the medical field. Each technology reviewed in this work aims to solve a unique problem with the current method or technology on the market. Some devices make powering implanted electronics easier, or even prevent surgeries to change a battery.

This work located seventeen journal or conference articles that pertain to this specific topic. After determining the most common MIMs, the papers were categorized into four groups: Implants, Pumps, Ultrasonic Imaging, and GI Endoscopy.

The transmission profiles from the experiments in each paper were analyzed and presented in Table 1. The results of each paper discussed their transmission efficiencies. The frequency, power, and coil distance were used to quantify and compare the efficiencies. Other quantifying criteria included coil size, topography and efficiency. With the results, it can be concluded that the theory of electromagnetic induction has feasible applications with medical implantable microsystems. Additional efforts to increase efficiency to the receiving coils are needed for further

implementation. Also, more government regulation is needed to keep the consumers safe and to provide uniform guidance to researchers and inventors.

Acknowledgements

NIH does not endorse or recommend any commercial products, processes, or services. The views and opinions of authors expressed herein do not necessarily state or reflect those of the U.S. Government nor does it constitute policy, endorsement or recommendation by the U.S. Government or National Institutes of Health (NIH). Please reference U.S. Code of Federal Regulations or U.S. Food and Drug Administration for further information. This project is sponsored by the NIH Center for Interventional Oncology grant.

CHAPTER 3

MODELING BIPOLAR RADIOFREQUENCY ABLATION WITH THERMOCHROMIC AGAR PHANTOMS

Introduction

Radiofrequency (RF) ablation therapy is a common modality to destroy cancer cells. Commonly, cancer of the breast, lung, kidney, liver, and others are treated with RF ablation. This procedure is minimally invasive and requires only a small catheter sized incision. Patients go through a computerized tomography (CT) scan for the physicians to be able to know what the position of a tumor is in the body. Then the physicians direct the ablation probes in the center of the tumor mass. This procedure is an alternative to other malignant neoplasms treatment modalities such as surgery or chemotherapy [77].

RF ablation utilizes two electrodes that direct electricity to flow between them. In RF tumor ablation, the resistive matter that separates the electrodes is the tumor tissue being ablated [78, 79]. When current flows between the electrodes through the tissue, the ions in that tissue will align in the direction of the current. However, when the current alternates at high frequencies, the ions will not be able to maintain alignment. Therefore, the ions will begin to vibrate and create frictional heat [80]. This process, called ionic agitation, is what heats a tumor to the cytotoxic temperature of 60°C, which eventually destroys those cells.

There are two types of radiofrequency ablation - monopolar and bipolar. Monopolar RFA has one electrode in the tumor while the other electrode, in the form of a grounding pad, is attached

to the patient's skin [12]. This method allows the heat to radiate outward from the electrode, uniformly. In bipolar RFA, both electrodes are inserted in the body and targeted to the tumor. This method heats and ablates the tissue directly between the electrodes [81].

During the procedure, the physician must know the zone of ablation which is exactly how much of the tumor is ablated. Many systems currently used for these ablation procedures advertise the potential ablation zones their equipment can create by publishing ablation zone charts [82, 83]. In this paper, the sizes and shapes of ablation zones will be compared as power and time change. To be able to create consistent structures to ablate, phantoms were made from agar powder. Agar powder is a natural compound found in algae [84]. This edible substance has coagulative properties, which makes the agar firm and able to be ablated.

Methods

In order to rapidly simulate the ablations, phantoms were created that have similar characteristics to human tissue. These phantoms are made from a salinated agar mixture with added thermochromic pigment to clearly display the ablation zone [85-87]. The agar powder used has a gel strength of 900g/cm², combined with a weak saline solution and irreversible thermochromic ink (ITP-BC60) [87].

12.5g	Agar powder
75.0mL	H ₂ O
0.385g - 0.400g	NaCl
0.100g	ITP-BC60

Table 3.1: Phantom Formula

To create the phantoms, 75ml of water, 0.385g - 0.400g of salt, and 0.100g of thermochromic ink(ITP-BC60) was added to a beaker and placed on a hot plate while using a

magnetic stirrer to constantly mix the solution (Table 3.1). When the mixture combined and its temperature was 40°C, 12.5g of agar powder was slowly added and stirred until the mixture reached 45-50°C. The mixture was then poured into the mold and placed in a -20°C freezer until the phantom solidified. Finally, the phantom was removed from the mold and then freezer and reached room temperature(15-20°C) before ablating.

The ablation generator used for the experiments in this work produces a 485kHz sine wave between two electrodes and can vary its power from 1-50 Watts. To keep consistent with commercial RF ablation generators, the operable impedance range was set from 50Ω to 330Ω [88, 89]. When the impedance exceeds the threshold of 330Ω, the values will be truncated only to display 330Ω.

The two electrodes were created from a 12 gauge hollow stainless steel rod. The electrode size of the can be determined using the surface area formula for a hollow cylinder (Eq. 3.1). The electrodes have an area of 101.8mm² and were placed 25mm apart for all ablation tests. Inside the rods are thermistors which indicate the temperature at that insertion point. In addition to the two ablation electrodes, two additional temperature probes were placed in the phantom - one to record the temperature of the center of the ablation zone, between the electrodes, and another on the side of the phantom to record its ambient temperature (Fig. 3.1).

$$SA_{electrode} = \pi dh = \pi * 2.70mm * 12.0mm = 101.8mm \quad (3.1)$$

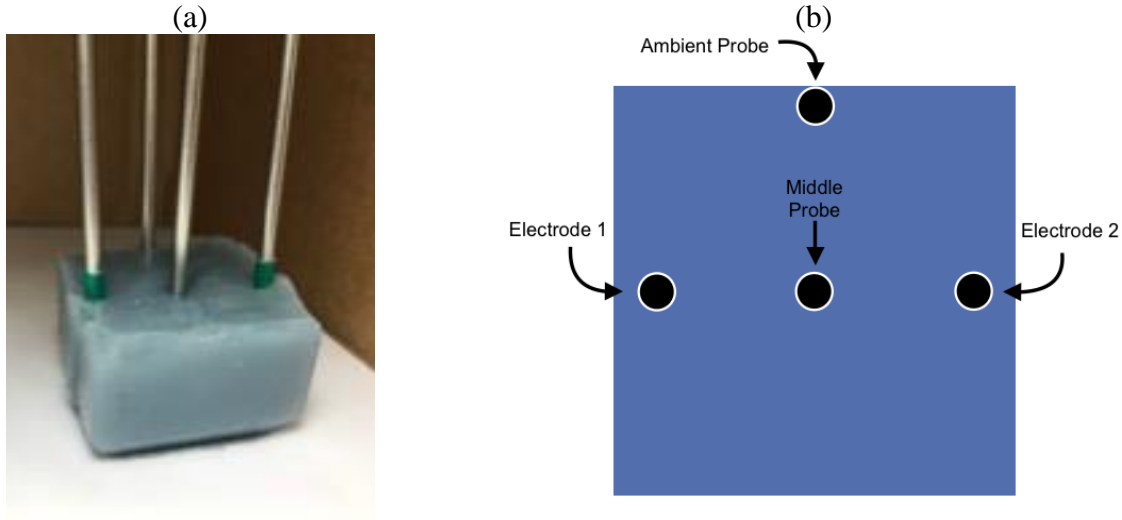


Figure 3.1. Ablation Setup

Experimental Results

Experiments were performed to determine the applicability of the agar phantoms for radiofrequency ablation testing. First, the initial impedances of phantoms were measured with varying amounts of salt in order to verify the consistency of the phantom impedance for the next tests. The change in impedance and temperature during ablation at different powers were characterized. Then, the final ablation zone was measured and the volumes were compared at each ablation power.

Initial Impedance Comparison

The amount of salt in the mixture has a direct correlation to the impedance of the phantom [90]. In order to determine the impedance of the phantom, several phantoms were made with varying amounts of salt. The same amounts of all the ingredients were formula was used (Table 3.1), just with different amounts of salt. Five different quantities of salt were tested - 0.100g, 0.200g, 0.300g, 0.400g, 0.500g. Each quantity was tested three times and the results were plotted

(Fig. 3.2). The results proved that the amount of salt and the total impedance have an indirect linear correlation. The more salt in the mixture, the less the total impedance will be.

In tumor ablations procedures, the impedance of human tissue ranges from about 75 to 150 Ω [11, 91]. Therefore, in order to recreate the same impedance with these phantom models, about 0.385g to 0.400g of salt should be added to the agar mixture. In the following tests, the impedance of the phantoms ranged from 90-120 Ω .

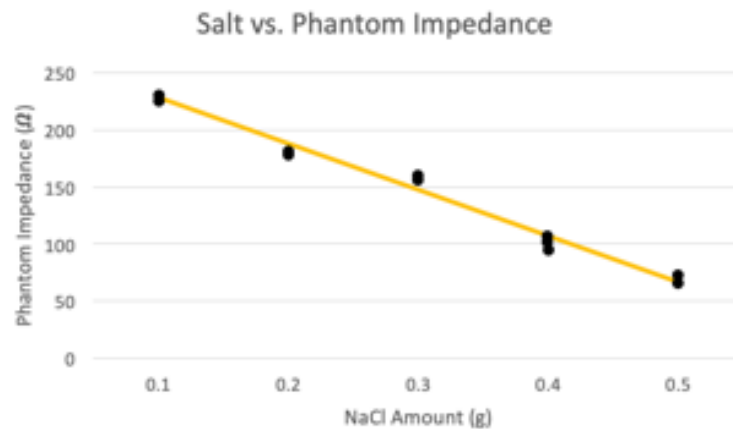


Figure 3.2. The relationship between the amount of salt in the mixture to the total phantom impedance.

Characterization of Impedance during Ablation

Ablations were performed on phantoms at powers of 10W, 20W, 30W, 40W, and 50W. During the ablations, the impedance was recorded and all plotted against time (Fig. 3.3). It was determined from the results of this test that power and ablation time had an inverse correlation. The higher the power, the shorter the ablation time was.

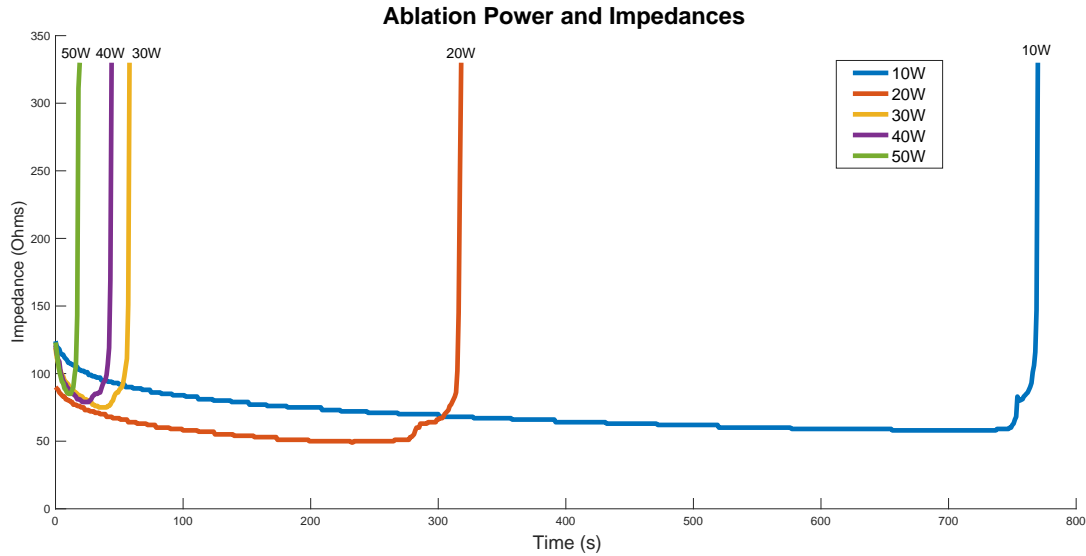


Figure 3.3. The impedance during ablation at every ablation power. The 10W ablation took the longest time at 770 seconds while the 50W ablation took only 19 seconds.

The impedances recorded at these different powers have the same curve characteristics. The impedance starts at about 100Ω , then gradually decreases by about 40Ω and has a spike in the impedance which ends the procedure. At the point where the electrode temperature reaches 100°C , the impedance begins to increase. When the water around the electrode becomes dry, the impedance spikes [10, 92, 93].

Characterization of Impedance during Ablation

Ablations were performed on phantoms at powers of 10W, 20W, 30W, 40W, and 50W. The initial temperature of the phantoms before ablation ranged from 14°C to 20°C and the ablation generator used produced a constant power of the value set. For each test, the impedance and temperature were recorded from 4 probes in the phantom. There is one probe in both electrodes, one probe was placed in the center of the phantom between the electrodes, and the last probe was placed on the side of the phantom to obtain the phantom's ambient temperature.

When comparing temperatures of all the different ablation powers, they also have similar characteristics. The temperature at the electrodes increases at a much faster rate than the other temperatures because the heat starts at the electrode. At lower powers, the temperature between the electrodes increases and reaches $\sim 60^{\circ}\text{C}$. At higher powers, the temperature at the electrodes reached 100°C faster, however, the temperature between the two electrodes was relatively unchanged.

In theory, both the electrodes would have the same temperature throughout the entire ablation procedure. However, in these tests, one of the electrodes was about 5°C hotter than the other. This difference increased the longer the phantom was ablated. Also, the difference between temperatures at the two electrodes was $\sim 20^{\circ}\text{C}$ at 50W. This phenomenon can be attributed to human error while creating the electrodes.

The thermochromic pigment in the phantom is irreversible and loses its blue color after the phantom reaches 60°C . Thus, making it possible to measure the ablated parts of the phantom. After each ablation, the phantoms were cut in half to examine the size of the ablation zone (Fig. 3.4).

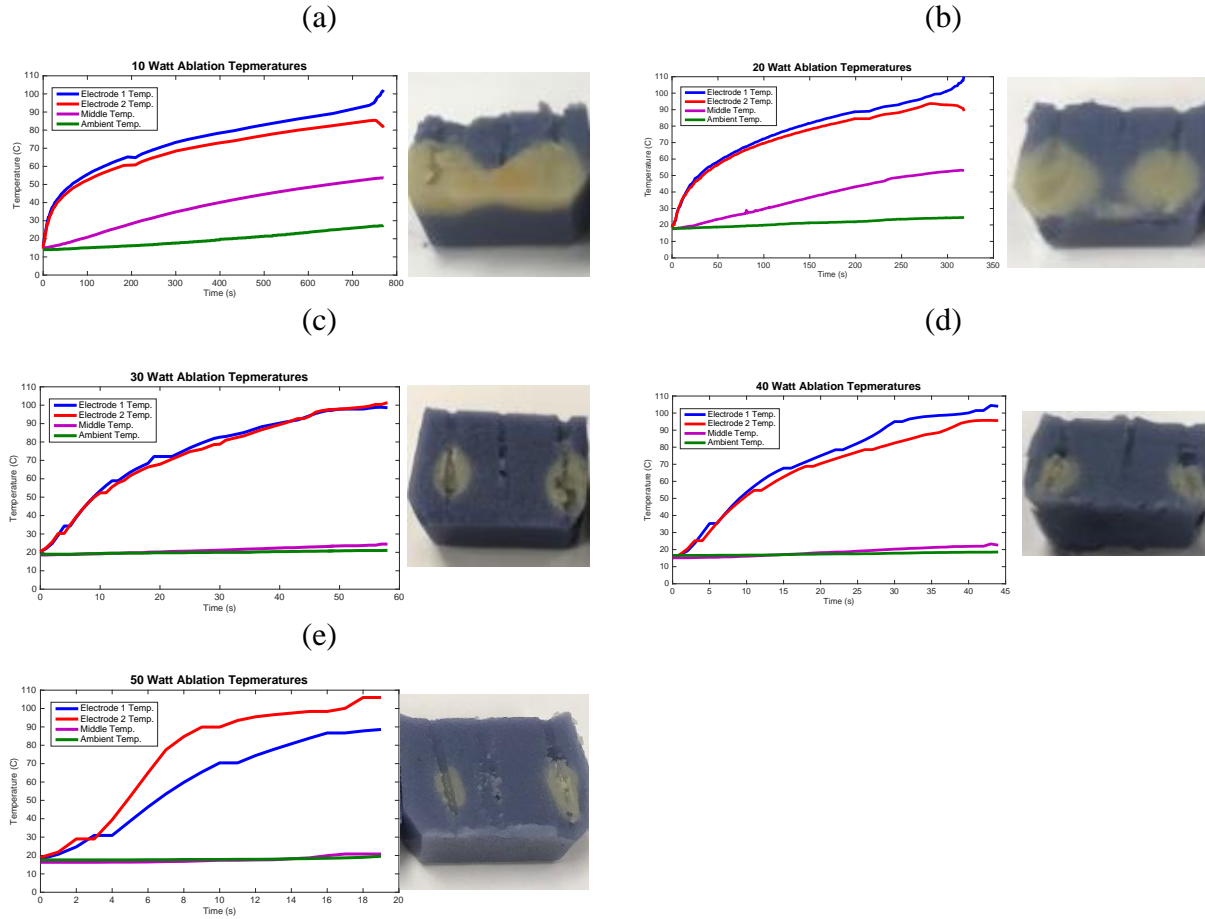


Figure 3.4. The phantom temperatures at the four probes during ablation at each power. The inside of each phantom after ablation showing the ablation zone

Conclusion

In this work, several phantoms were created to mimic the characteristics of human tissue during ablation. The tests were based on specific controls; the electrodes had a surface area of about 100 mm^2 and the distance between them was 3 cm. These phantoms, made from a saline and agar powder mixture, were tested to determine the ablation zone at different powers while their impedance and temperature were monitored. It was determined that as power increased, the ablation time and ablation zone volume decreased. Thus, the largest ablation zones were created when the power was low and more of the phantom could increase to the ablation temperature of 60°C .

This study provided a thorough analysis of how agar phantoms can be used under specific controls. More work can be done to test how the phantoms perform at different electrode distances and electrode sizes. Also, conducting the same tests on animal tissue, can help to further compare the phantom to current methods of tumor ablation.

CHAPTER 4

DEVELOPING A RADIOFREQUENCY TUMOR ABLATION SYSTEM WITH WIRELESSLY POWERED CATHETER

Introduction

Ablation therapy is a medical procedure that can treat several different problems in the body. Some of these procedures include cardiac ablation for the treatment of atrial fibrillation and lateral branch neurotomy for chronic sacroiliac joint pain treatment [94-96].

Tissue Ablation is a minimally invasive medical procedure in which tissue, most commonly, cancerous or benign tumors, are destroyed. Ablation appeals to many patients that are not candidates for resection because they are highly invasive and can pose great risks. Ablation only requires needle sized incisions rather than the larger incisions required for a laparotomy. In most modalities, the tissue is heated or cooled to cytotoxic temperatures with several different types of energy. Cryoablation uses extreme cold to ablate while microwave, radiofrequency, high intensity focused ultrasound (HIFU), laser ablation, and others use heat to ablate [97-100]. In thermal ablations, temperatures above 60°C will cause destruction at the cellular level, leading to cell death[8].

Radiofrequency ablation is commonly used to treat lesions in the liver, kidney, lung, bone, breast, prostate and pancreas [6, 7]. This method uses electrical current that alternates at radio frequencies between two electrodes [8-10]. The probe is inserted into the body and contacts the part of tissue the operator wishes to ablate. The tissue introduces a resistance and completes a

circuit between the two electrodes. Then when current is applied, the ions in the tissue align in the direction of the current. When that current alternates, the ions agitate, causing tissue coagulation, and thus resulting in cell death [11, 12].

In monopolar RFA, one electrode will be inserted into the body on a catheter and the other electrode is a grounding pad contacting the skin usually on the legs of the patient. The ablating electrode or electrodes that are inserted into the lesion radiate heat outward uniformly because there is significant distance to the dispersion electrode [101]. In bipolar RFA, both electrodes are inserted into the body and the current flows between them. This method ablates the tissue directly between the electrodes in the tissue. When the electrodes have an equal surface area, the current density in that region will be uniformed. However, if the electrode sizes are unequal and the current remains the same, the current density will be greater around the electrode with the smaller surface area [101, 102].

In practice, there are three methods to perform these RFA ablations – percutaneously, laparoscopically, or by laparotomy. Percutaneous ablations are generally outpatient procedures conducted with contrast-enhanced computerized axial tomography (CT) guidance and sometimes accompanied with live fluoroscopy or ultrasonography. Percutaneous RFA can be performed under general or local anesthesia, while laparoscopic and laparotomic RFA requires general anesthesia. Ablations performed percutaneously have less negative effects and can be performed quickly, however visualization is limited [102, 103].

Laparoscopic ablations utilize enhanced imaging with endoscopic cameras and/or ultrasound transducers placed on the surface of the organ. While increased visualization can lead to more accurate staging and ablation, probe placement is difficult since probes must enter through a laparoscopic port. The laparoscopic approach is more invasive than the percutaneous method

and may require overnight hospitalization [103-105]. Laparotomic RFA is often performed while resecting larger tissue. In this method, small tumors may be precisely ablated but is still a highly invasive procedure and requires additional recovery time [102, 103].

Current percutaneous tumor ablation procedures are usually performed in an operating room equipped with a Fluoroscopy CT scanner. These operating rooms also have anesthesia and patient monitoring equipment. A number of equipment and cables may be tethered to the patient, which could limit the workflow efficiency. The weight of the ablation cables could also alter the needle location when the physician lets go of them.

During the procedure, there are several people in the operating room, including the interventional radiologist who performs the ablation, one to two imaging technologists, an anesthesia nurse, and sometimes a representative from the ablation device company. Therefore, the operating room is very busy environment it is possible that someone could trip on one of these chords in the operating room.

In the methods presented in this manuscript, bipolar RFA will be utilized, thus both electrodes will be connected to one catheter. Additionally, the intended use for this work is to be performed in percutaneous procedures. The prototype presented in this manuscript aims to prove the concept of performing radiofrequency ablation procedures using electromagnetic induction.

Methods

Inductive power transfer theory was used to wirelessly deliver power to the ablating electrodes. The Ampere-Maxwell Law states that electrical current flowing through a coil of wire

creates a magnetic field around that wire. In addition, when that electrical current alternates in the wire, there will be an alternating magnetic field (eq. 4.1) [15, 106-108].

$$\oint \vec{B} d\vec{l} = \mu_0 \left(I_{enc} + \varepsilon_0 \frac{d}{dt} \int_S \vec{E} \cdot \hat{n} da \right) \quad (4.1)$$

The Law of Biot-Savart (eq. 4.2) is applied to determine the strength of that magnetic field at any height from the center point of the transmitting coil. Since the coil used is a symmetrical circle the surface integral about the line equals one and the equation reduces to a function of current and circle radius [15, 106-108].

$$B = \frac{\mu_0 I}{4\pi R^2} \oint dL = \frac{\mu_0 I}{2R} \quad (4.2)$$

Faraday's Law of Induction states that an electromotive force will be induced on a coil of wire placed into a changing magnetic field. This law is representing the relationship between the strength of the magnetic field (flux), the area of the coil and the number of turns in that coil (eq. 4.3) [15, 106-108].

$$\varepsilon = -N \frac{\Delta \Phi_B}{\Delta t} \quad (4.3)$$

The frequency of the oscillations can be modified by changing the inductance of the coil or the capacitance of its tuning capacitor in the LC tank circuit. The receiving coil has a similar LC tank circuit to the transmitting circuit. The inductors and capacitor are tuned to be in resonance with each other. Magnetic resonance relates the operating frequency to the values of the capacitor and inductor used. When the LC circuit operates at this the resonant frequency its reactance is its highest and its impedance is at its lowest point. Therefore, the power at the resistive load will high. The formula to determine the resonant frequency in this parallel tank circuit is shown in equation 4.4 [15, 106-108].

$$f_{resonant} = \frac{1}{2\pi\sqrt{LC}} \quad (4.4)$$

The ablation system is comprised of two parts; the ablation generator which has an oscillating circuit and transmitting coil. Then, the wireless catheter has the receiving coil and the catheter that is intended to be inserted in the body and ablate tissue. The ablation generator creates a magnetic field while the wireless catheter has a coil of wire that is placed into that field. Figure 4.1 shows how the two parts of the system are used together.

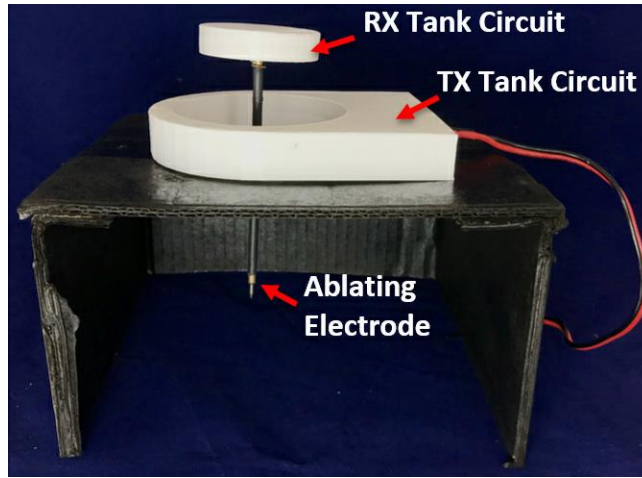


Figure 4.1. Diagram of the Ablation System. The wireless catheter consisting of the RX tank circuit and ablating electrode is inserted through the TX tank circuit.

Ablation Generator

The ablation generator uses an amplification circuit to create an alternating current through a coil to create an alternating magnetic field. A modified Royer amplifier was used to create a medium power alternating current. The Royer amplifier is advantageous when the coil distances are intended to be changed because the oscillation frequency is related to the resonant frequency of the transmitting and receiving tank circuits. Therefore, the oscillating frequency will change as the coil distance varies.

The amplifier utilizes two MOSFETS that are cross coupled and connected to the LC tank circuit. Once the gate of one of the MOSFETS is triggered it opens its switch and allows current to flow from the drain to the source. This also forces the gate voltage of the other MOSFET to zero which turns that switch off thus only allowing one MOSFET to be on at one time[15]. Figure 4.2 shows the gate voltage(V_{GS}) of one MOSFET and the drain voltage(V_{DS}) of the cross coupled MOSFET.

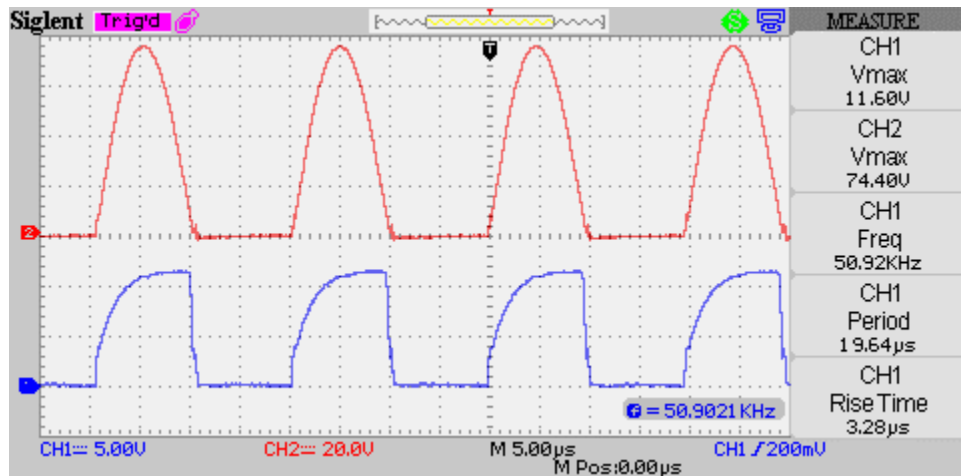


Figure 4.2. Time Domain Analysis of V_{GS} and V_{DS} of the cross coupled MOSFET. Channel 1 is bottom waveform which is V_{GS} and channel 2 is the top waveform is V_{DS} of the cross coupled MOSFET.

The circuit is powered from a 12-24V adjustable power supply with a maximum DC current of 2.5-amps. The LC tank circuit is designed in a parallel configuration with its characteristics defined in Table 4.1. With equation 4 and the values of the LC tank circuit, a frequency of 50.5kHz is calculated. This value was validated in practice as an oscillating frequency of 50-55kHz was observed. This circuit amplifies the natural oscillating feedback of the LC tank circuit to create a strong magnetic field through the coil [109, 110]. Figure 4.3 shows the diagram of the modified Royer circuit used to amplify the oscillations of the tank.

Inductance	25.74 μ H
Capacitance	386.3nF
Coil Diameter	10-cm
Coil Turns	12

Table 4.1: TX Tank Circuit Characteristics

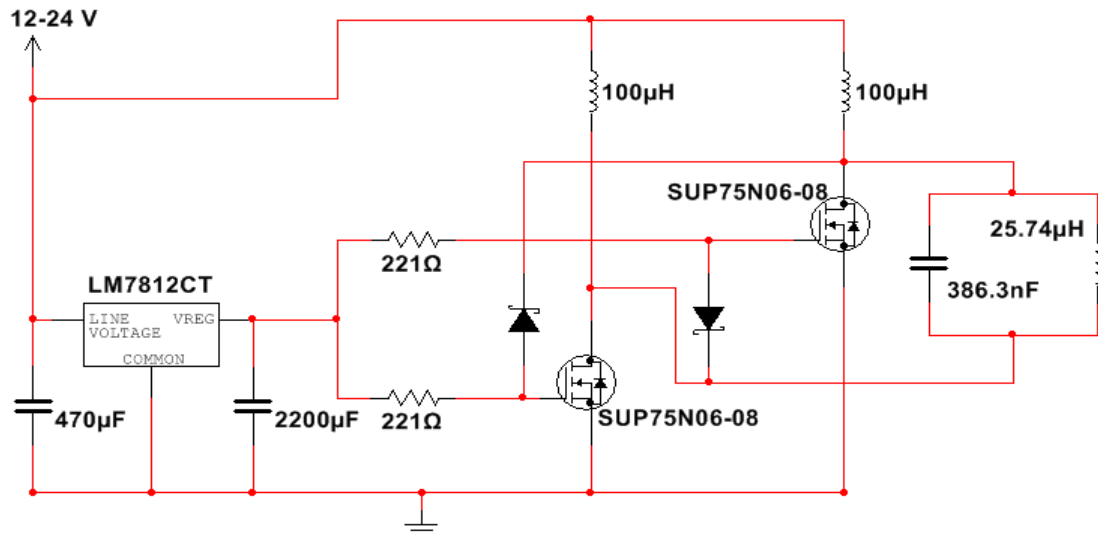


Figure 4.3. Circuit Diagram of the Transmitting(TX) Circuit

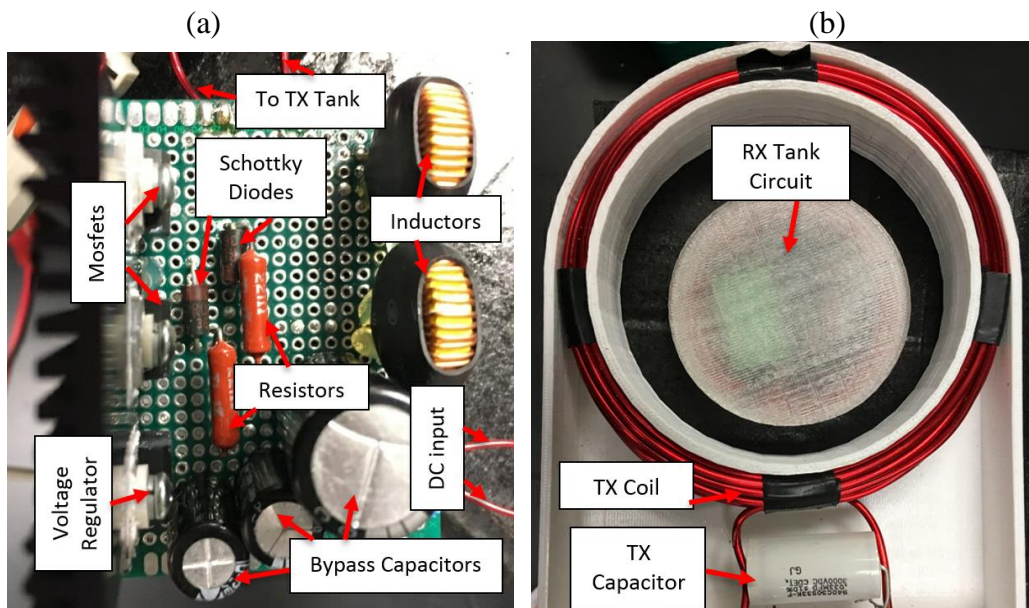


Figure 4.4. Photo of the (a) TX circuit and (b) TX and RX tank circuit

Wireless Catheter

While the ablation generator produces an oscillating magnetic field, the receiving coil connected to the wireless catheter is placed within those flux lines and a voltage is induced (eq. 3). The receiving LC tank circuit is half the diameter of the transmitting and has a parallel configuration that is in resonance with the transmitting circuit (Table 4.2).

Inductance	25.69 μ H
Capacitance	400.2nF
Coil Diameter	5-cm
Coil Turns	14

Table 4.2: TX Tank Circuit Characteristics

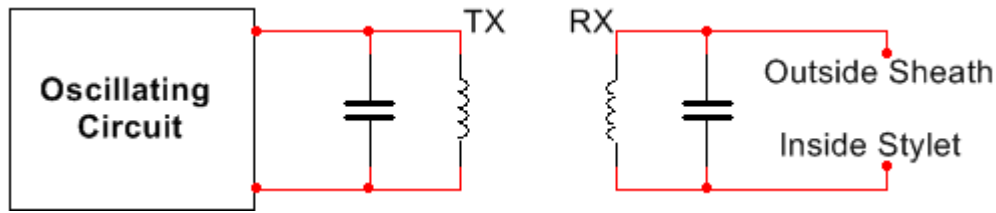


Figure 4.5. Diagram of the Transmitting(TX) and Receiving(RX) Circuits

The catheter selected to be used in this work is 6.5 gauge and is 12 cm in length. The catheter is constructed in two parts - the inside stylet and the outside sheath. Each part is connected to one side of the receiving LC circuit as shown in figure 4.5. These two parts are insulated from each other in order to only allow current to flow from the electrodes through the load.

The surface area of the electrodes is important to consider in order to predict and understand the ablation zone the catheter creates. The geometry of the inside stylet electrode is comprised of a hollow cylinder and a cone. Therefore, the surface area of this electrode is represented by equation 4.5. The surface area of the inside stylet electrode was calculated to be 67 mm².

$$SA_{inside\ stylet} = \pi d_{cyl} h_{cyl} + \frac{\pi d_{cyl}}{2} \sqrt{\left(\frac{d_{cone}}{2}\right)^2 + (h_{cone})^2} \quad (4.5)$$

The geometry of the outside sheath electrode is comprised of a hollow cylinder and its circular base that is represented as an annulus. Therefore, the surface area of this electrode is represented by equation 4.6. The surface area of the outside sheath electrode was calculated to be 79 mm².

$$SA_{outside\ sheath} = \pi d_{cyl} h_{cyl} + \pi \left(\left(\frac{d_1}{2} \right)^2 - \left(\frac{d_2}{2} \right)^2 \right) \quad (4.6)$$

The catheter was constructed so that the surface area of the outside sheath electrode was 18% larger than the inside stylet electrode (fig. 4.6). This difference in surface areas directs the ablation zone toward the electrode with the smallest electrode surface area [101, 111]. In this case, the electrode with the smaller surface area is the inside stylet electrode, therefore the ablation zone is closer to the tip of the catheter.

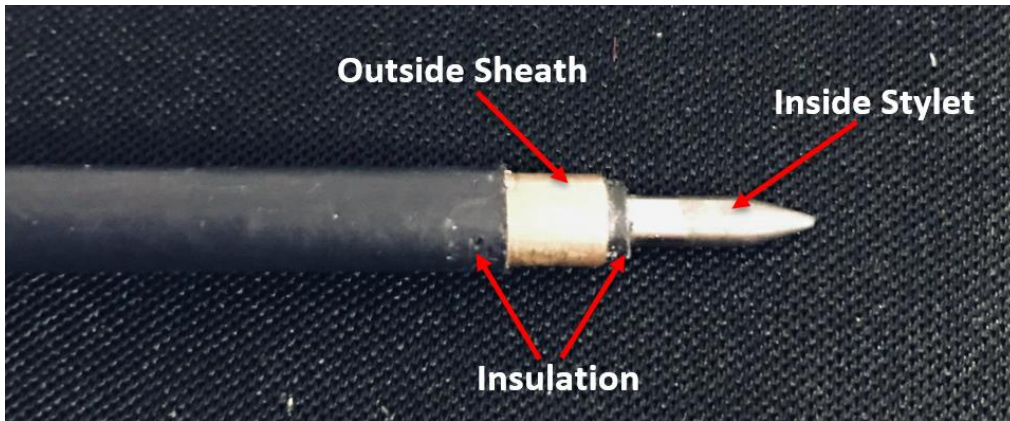


Figure 4.6. The tip of the ablation catheter prototype

A thermistor is also inserted into the hollow catheter to measure the temperature at the tip of the catheter during ablation. The thermistor is connected to a small battery powered circuit that allows the catheter to be completely independent from any wired source.

Experimental Results

Four experiments were performed to evaluate the performance of the ablation system. The first and second tests directly focus on the efficiency of the wireless power transfer. A resistor is connected to the RX coil and power is measured as the distance between the coils increase and as the input DC voltage changes. Then, the third test is to ablate ex vivo bovine tissue to evaluate the feasibility of this ablation system. For these experiments, the wireless catheter was connected in parallel to a load, either a resistor or animal tissue. This setup is represented by the circuit diagram found in figure 4.7 and figure 4.8.

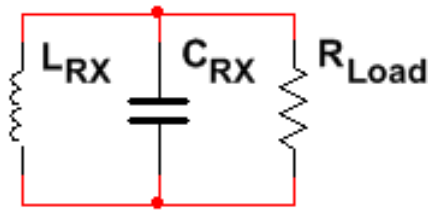


Figure 4.7. Diagram of the Receiving(RX) Circuit during testing and ablation

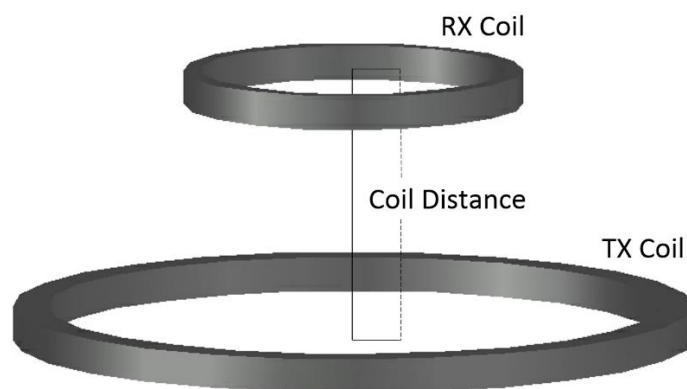


Figure 4.8. Diagram of the distance between the TX and RX Coils

Coil Distance and Power Efficiency with Resistive Load

The power of the ablation system was measured at the transmitting and receiving side to determine the efficiency of the wireless power transfer while the distance between the coils increased. In this experiment, a purely resistive load was added in parallel with the receiving tank circuit. The resistor was measured to be 103.1Ω . During this experiment the power received and its corresponding power efficiency at each coil distance will be observed. The distance between the coils is negatively proportional to the catheter insertion depth; as the catheter depth increases, the distance between the coils decrease.

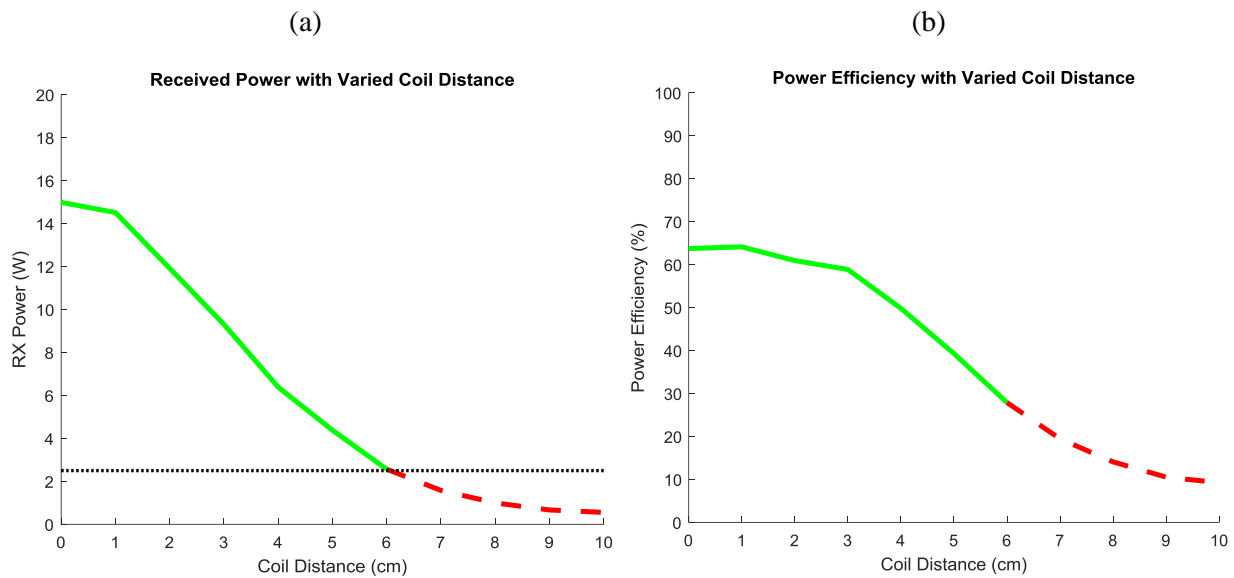


Figure 4.9. Received power and efficiency as coil distance increases (a) Average received power for 3 trials, Distances at or below 6cm are above the 2.5W ablation minimum, (b) Average received power efficiency at each coil distance for 3 trials

These tests were performed at a DC input voltage of 24 VDC, where the maximum transmitting power is possible. Three trials were conducted at each distance to determine the received power and efficiency. The mean of the received power and efficiency for the trials is shown in red in figure 4.9. The largest received power and efficiency was achieved when the coils

are at a contact distance. A maximum of 15W was recorded at the load when the coils were at contact distance. As the coil distance increased, the received power and efficiency decreased. The minimum desired RX power is 2.5W, powers less than this take extremely long to ablate with the presented catheter. Thus, a 6cm coil distance is indicated as the maximum working distance.

Received Power and Varying DC Input Voltage with Resistive Load

When the presented ablation system is in use the only variables able to be manipulated are the catheter insertion depth and the DC input voltage. This experiment aims to determine the received power and the corresponding power efficiency as the DC input voltage varies. The operational voltage for the DC input ranges from 12VDC to 24VDC. In this experiment the power and efficiency were measured at increments of 1VDC.

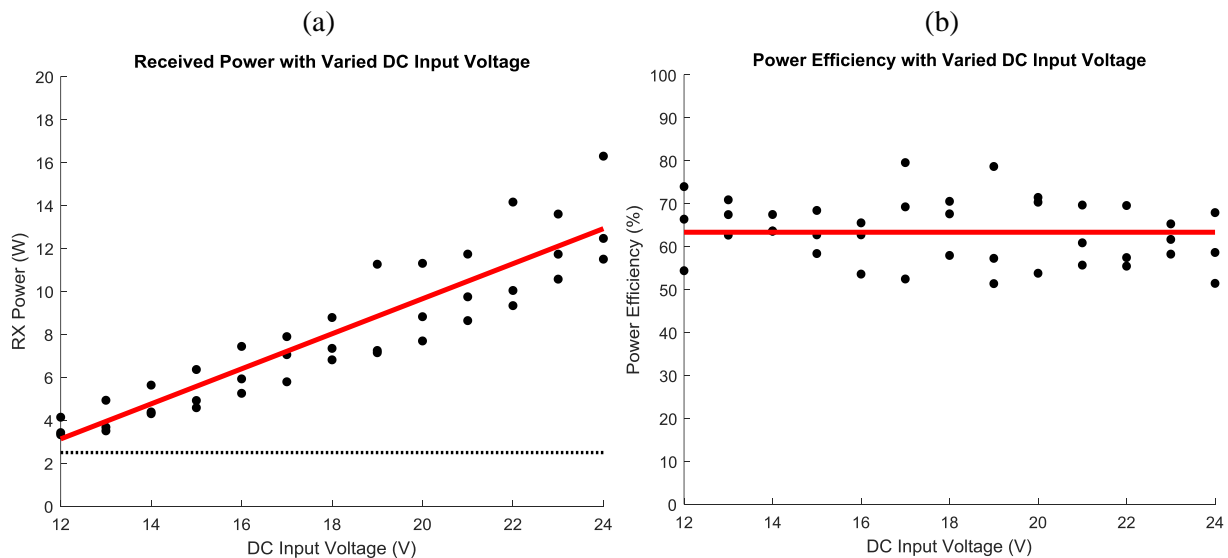


Figure 4.10. Received Power and efficiency as DC input voltage increases (a) Average received power for 3 trials, all above the 2.5W ablation minimum, (b) Average received power efficiency for 3 trials, 63.27%

Since the coils remained at contact distance during these tests, the mutual inductance of the two tank circuits also stayed the same. Therefore, the efficiency was nearly the same for each regardless of the DC input voltage. The average efficiency recorded for all tests was 63.27% and the power received increased linearly as the DC input voltage increased (Fig. 4.10).

Ex Vivo Bovine Tissue Experiment

In this experiment, ex vivo bovine tissue was obtained to observe how the presented ablation system ablated tissue (fig. 4.11). Two tests were conducted – one with maximum ablation power and one with minimum ablation power. The temperature was recorded with the thermistor circuit on the wireless catheter. This tissue had an initial impedance of about $175\ \Omega$ for all tests. The temperature of the tissue was monitored while the ablations were performed.

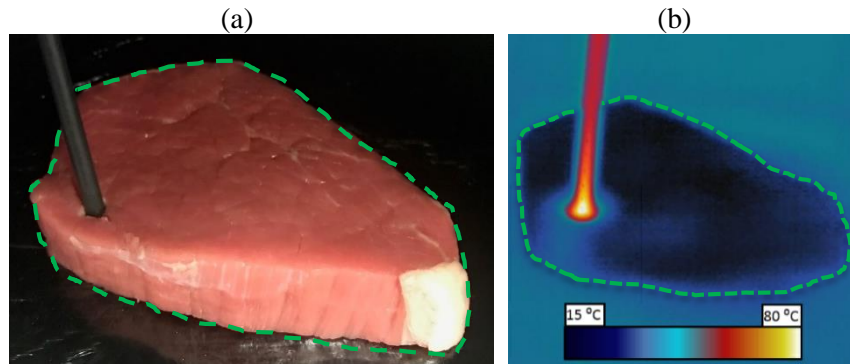


Figure 4.11. Setup of the bovine tissue experiment (a) ex vivo bovine tissue before ablation, (b) tissue during ablation

Maximum Power

The first test was ablation at 24VDC with the coils at contact distance. 3 trials were conducted for 2 minutes and the temperatures during ablations were plotted over time (Fig. 4.12b).

From this data, a consistent temperature rise and decay was observed for each trial. The ablation zones were also nearly the same with a width of 9 mm and a length of 18 mm (Fig. 4.12a).

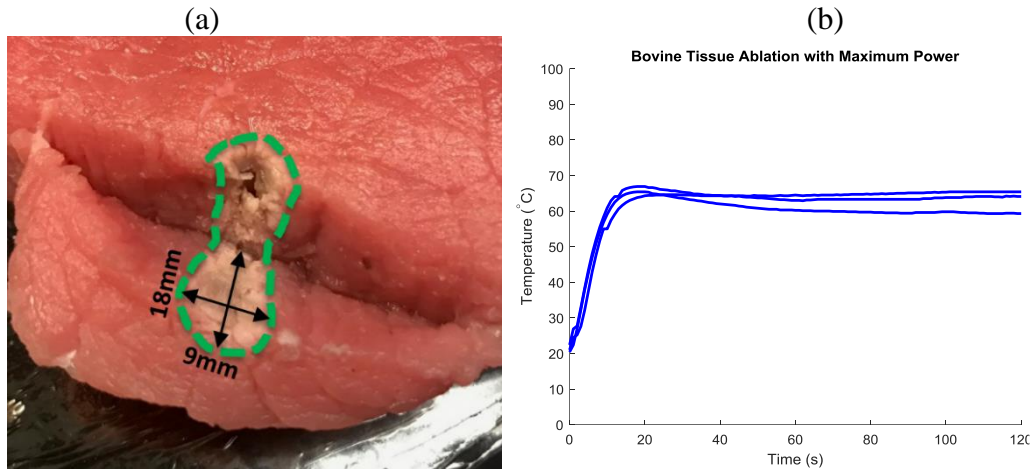


Figure 4.12. Results of Maximum power test. (a) cross section of ablation zone. 9mm x 18mm, (b) ablation temperatures over time

Minimum Power

The next test was ablating the tissue at its minimum powers. This is achieved with an input voltage of 12 VDC at 0 cm coil distance and an input voltage of 24 VDC at 6 cm coil distance. The tissue was ablated for 5 minutes in each case and their temperatures during ablation were plotted over time (Fig. 4.13b). From the temperature data, the 12 VDC ablation had a faster rise in temperature because the power was slightly higher. The ablation at 6 cm distance had a lower power because the temperature rise was slower. However, the ablation zones for both tests were nearly the same with a width of 12 mm and a length of 21 mm (Fig. 4.13.a).

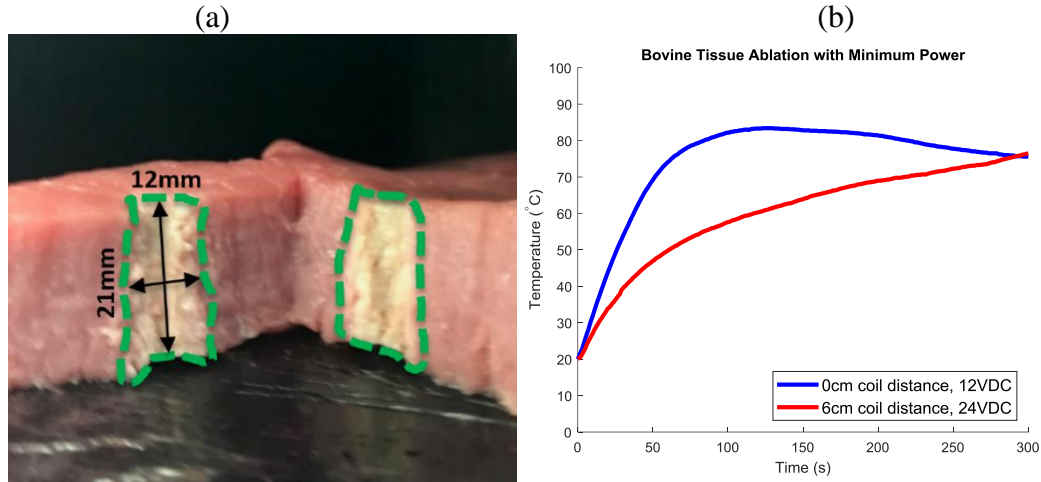


Figure 4.13. Results from the minimum power test. (a) cross section of ablation zone, 12mm x 21mm, (b) ablation temperatures over time

Conclusion

Ablation therapy is a method used to treat several conditions within the body including cancerous and benign tumors. Tumor ablation can be achieved with many types of energy by bringing the tissue above the cytotoxic temperature of 60°C. Radiofrequency ablation uses alternating electrical current to ablate tissue by agitating their ions.

A bipolar radiofrequency ablation system was developed to investigate the possibility of ablating tissue wirelessly. The system is comprised of the ablation generator and wireless catheter. The generator is comprised of an oscillating circuit that creates a medium power magnetic field. The catheter has a receiver coil that is induced with a voltage when placed in that magnetic field. The catheter has 2 electrodes that allow alternating current to flow through tissue.

To test the performance of this ablation system, tests were conducted to observe its received power, temperature, and ablation size. The average maximum received power was 15W where an average maximum efficiency of 63.27% was recorded. The ablation power and temperature was tested using ex vivo bovine tissue. The system was able to ablate up to a 2 cm ablation zone. With

these results, the concept of using inductive power transfer to perform radiofrequency ablation wirelessly was proven.

The prototype ablation system outlined in this work is the intended to prove the concept of wireless ablation. More work can be done to further improve the system. The efficiency of the power transfer can be increases by using a more robust amplifier with less resistive losses. Additionally, more tuning may be needed in order to increase the coupling between the two coils. Also, experiments should be conducted to evaluate the size of the ablation zone with electrodes of different surface areas and spacing.

Acknowledgements

The authors would like to give a special thanks to Dr. Mark Haidekker for helping perfect the Royer circuit schematic and building the version used in this chapter.

NIH does not endorse or recommend any commercial products, processes, or services. The views and opinions of authors expressed herein do not necessarily state or reflect those of the U.S. Government nor does it constitute policy, endorsement or recommendation by the U.S. Government or National Institutes of Health (NIH). Please reference U.S. Code of Federal Regulations or U.S. Food and Drug Administration for further information. This project is sponsored by the NIH Center for Interventional Oncology grant. This study was also supported in part by the National Institutes of Health (NIH) Bench-to-Bedside Award, the NIH Center for Interventional Oncology Grant, the National Science Foundation (NSF) I-Corps Team Grant (1617340), NSF REU site program 1359095, the UGA-AU Inter-Institutional Seed Funding, the American Society for Quality Dr. Richard J. Schlesinger Grant, the PHS Grant UL1TR000454 from the Clinical and Translational Science Award Program, and the NIH National Center for Advancing Translational Sciences.

CHAPTER 5

BATTERY POWERED WIRELESS TUMOR ABLATION SYSTEM AND PROPOSED FUTURE WORK

Introduction

Current percutaneous tumor ablation procedures are usually performed in an operating room equipped with a Fluoroscopy CT scanner. These operating rooms also have anesthesia and patient monitoring equipment. A number of equipment and cables may be tethered to the patient, which could limit the workflow efficiency. The weight of the ablation cables could also alter the needle location when the physician lets go of them. During the procedure, there are several people in the operating room, including the interventional radiologist who performs the ablation, one to two imaging technologists, an anesthesia nurse, and sometimes a representative from the ablation device company. Therefore, the operating room is very busy environment it is possible that someone could trip on one of these chords in the operating room.

This work aims to evaluate the possibility of using wireless power to ablate tissue. The ablation device presented in Chapter 4 utilizes a wirelessly powered ablation catheter. The transmitting circuit used is powered by a fixed power supply. This produces a controlled environment for analysis of the electrical characteristics including power efficiency. However, in practice, the power supply still restricts the functionality of the system and it is not truly wireless. This chapter introduces a similar wireless ablation system that has a battery powered generator.

Thus making the ablation system completely wireless during the ablation procedure. In this chapter, other iterations of the wireless ablation system are also presented.

Methods

As outlined in chapter 4, electromagnetic induction was used to power an ablation catheter wirelessly. A coil of wire is needed to oscillate with enough power to produce a magnetic field and induce an electrical current on the receiving coil centimeters away. The Law of Biot-Savart (eq. 4.2) was applied to determine the strength of the magnetic field at any height from the center point of the transmitting coil. Since the coil is a symmetrical circle the surface integral about the line equals one and the equation reduces to a function of current and circle radius. Placing another coil of wire within this switching magnetic field will generate an electrical current that will be directed through a tumor in the body.

Transmitting Circuit

A transmitter was built equipped with an oscillating circuit and resonating coil (Fig. 5.1). The circuit oscillates at ~215 kHz and generates a sine wave. The circuit is powered by a 32 VDC lithium ion battery source and requires up to 3 amps DC to generate the sine wave without a load on the receiving side. The current transmitting coil is 12 cm in diameter, has 3 turns, and has parallel capacitance to tune its resonant frequency.

The electrical components and transmitting (TX) coil will be embedded into a portable wireless RFA generator (Fig. 5.2). The electronics will be powered by a battery so the entire system will be wireless. There is a square hole cut into the RFA generator where the receiving catheter

will operate. Constricting all the electronics to this enclosure will provide a clean workspace for the operating surgeons.

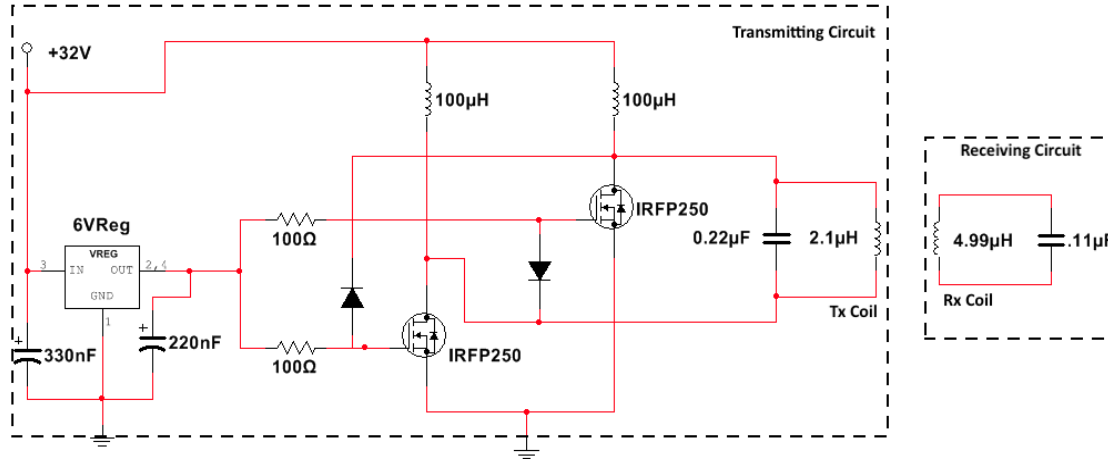


Figure 5.1. Transmitting Circuit Diagram

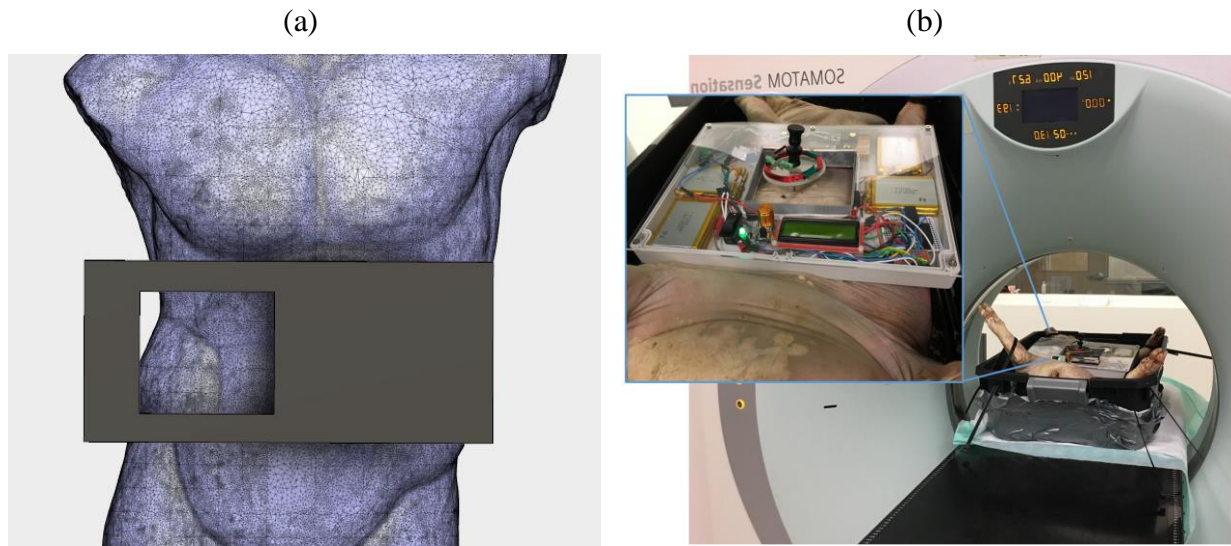


Figure 5.2. Ablation generator with all electronics embedded. (a) CAD drawing of the ablation generator. (b) The ablation generator in use on a porcine cadaver in a CT scanner.

Receiving Circuit

The catheter was constructed with two parts – the inside stylet and the outside sheath (fig. 5.4). The inside stylet has a diameter of 0.85 mm and the outside sheath has a diameter of 1.75

mm. Each were connected to one side of the receiving coil as represented in figure 4.5. The receiving coil was coupled at the same resonant frequency in order to receive the largest voltage. First, the inductor coil was made to be 6 cm, half the diameter of the transmitting coil. Then a capacitor was added to couple the transmitting coil and receiving coils using equation 4.4.

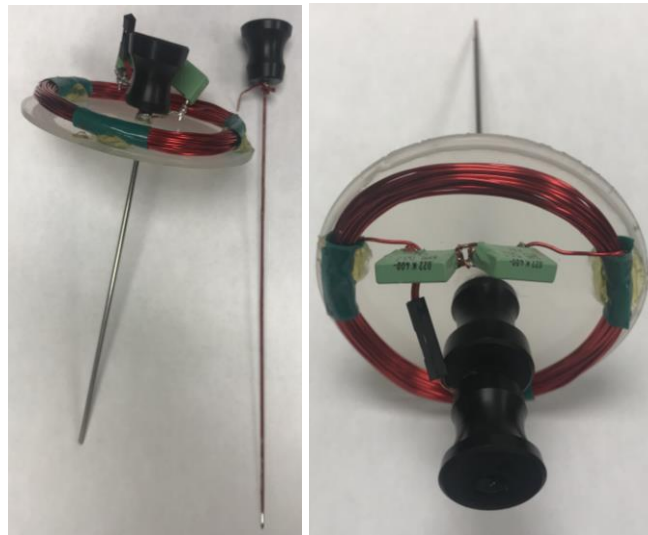


Figure 5.3. The ablation catheter prototype. The left image shows the inside needle next to the outside sheath and the RX LC Circuit. The right image shows both parts of the catheter together.

The inside stylet was coated with insulating varnish to prevent the two parts from touching and shorting the circuit. The base of the catheter was not coated so that a wire could connect to the receiving coil (fig. 5.3). 1 mm length of the tip of the catheter was also not coated to allow the current to flow through the tissue and back to the outside sheath (fig. 5.4).

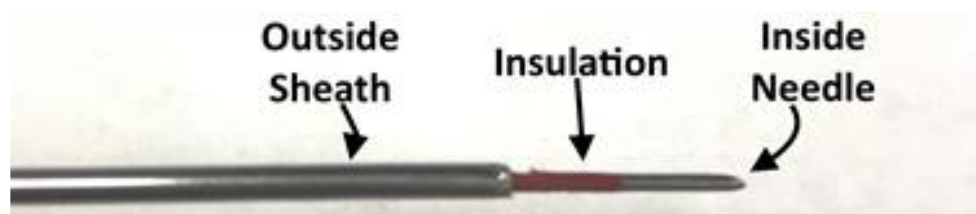


Figure 5.4. The tip of the ablation catheter prototype. The inside needle is inserted into the outside sheath and the varnish insulates the inside needle from the outside.

Experimental Results

The prototype catheter was tested to see if the ablation system could ablate tissue within the body. Porcine tissue was used to simulate the functionality of the prototype system and to observe the heat dissipation through sample tissue.

For each ablation area tested, the catheter was inserted for 60 seconds. The catheter was positioned in the center of the transmitting coil and kept at depth of 10–12 cm. With the visual and thermal results (fig. 5.5), it was determined that the catheter was able to ablate a 2 cm sphere around the tip.

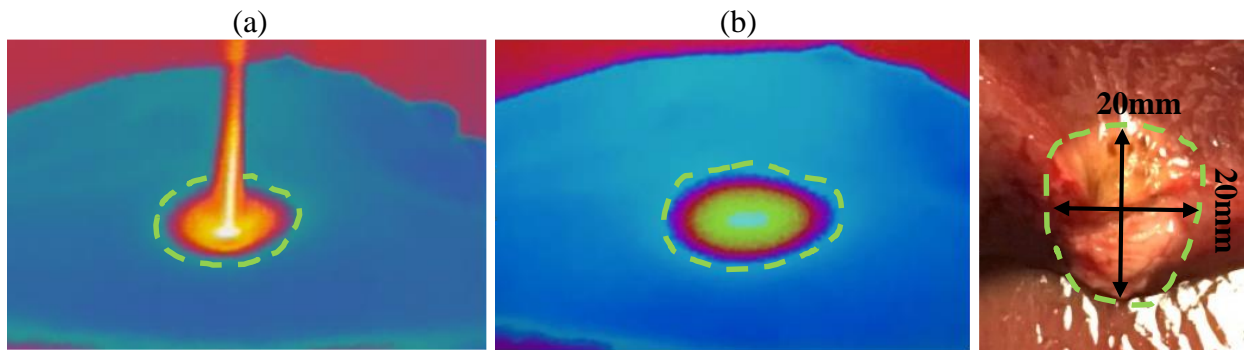


Figure 5.5. Results from ex vivo porcine liver test (a) thermal image during ablation, (b) thermal image after ablation (c) image of the 2cm sphere of ablation

Conclusion and Future Work

A prototype system was developed to wirelessly transfer energy to the tip of an ablation catheter. A transmitting coil was resonantly coupled with a receiving coil connected to separate parts of the catheter. The catheter was also used to perform the ablation procedure with a pig liver. In this experiment, the catheter was able to generate heat at the liver tumor target, resulting in a 20 mm spherical ablation volume. Performing thermal ablation wirelessly was proven to be a feasible alternative to the traditional wired approach. In this chapter, another prototype was presented. Instead of powering the system with a power supply as done in chapter 4, this prototype is battery powered. This battery powered system is completely wireless during the procedure and is portable.

Future work includes further development of the transmitting circuit enclosure. The design can be improved to include a microcontroller to monitor and control the ablation time. The ablation catheter prototype can be further refined to make the receiving coil smaller in diameter to make the catheter easier to hold. A cooling element and thermal couple might be able to be integrated in the catheter design to ensure the RFA is performing in a well-controlled manner. The next generation of the prototype can be fully integrated with a CT scanning table in order to streamline the ablation and imaging process. A drawing of a possible design is show in figure 5.6. Further testing is required to ensure compatibility with computed-tomography (CT) imaging.

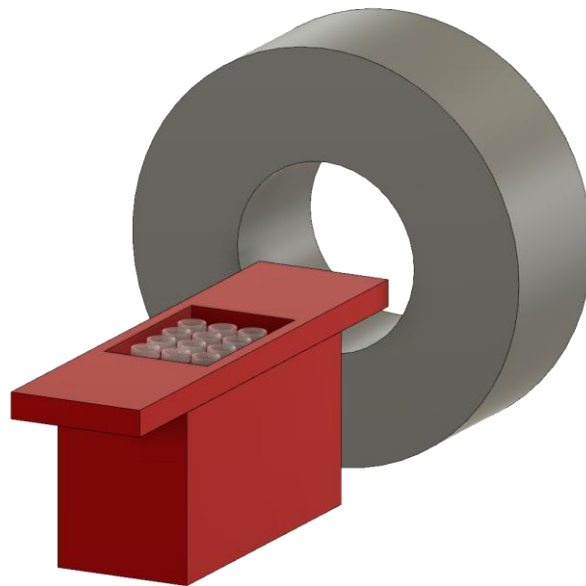


Figure 5.6. Proposed next generation prototype which has an array of transmitting coils embedded into a CT scanning bed.

CHAPTER 6

CONCLUSION

Theories relating electricity and magnetic field were first written in the late 19th century. In the last few decades, more industries use these theories of wireless power transfer in their portable devices, mostly to charge batteries. Throughout this work, the use of wireless power transfer in the medical device field was observed. First, the field of wirelessly powered medical devices was studied. The literature review in chapter 2 shows how the medical field is currently using wireless power. 247 published manuscripts were searched through and 17 manuscripts were identified as the most relevant and innovative. Then, the papers were categorized into four groups: Implants, Pumps, Ultrasonic Imaging, and GI Endoscopy.

Second, bipolar radiofrequency ablation was examined with ablation phantoms. The phantoms were made from agar powder, thermochromic pigment, and a saline solution which made ablation testing consistent and easily reproducible. Two electrodes of equal surface area were placed in these phantoms at a fixed distance and ablated. The ablations were performed while time, temperature, impedance, and its final ablation zone were examined. With the controls defined in the experiments, it was found that as power increased, the ablation time and ablation zone volume decreased. Therefore, the larger ablation zones were created with lower powers.

The principles of bipolar radiofrequency examined were used to create a new ablation system. This system utilizes wireless power transfer to heat tissue at the tip of its catheter wirelessly from the generator. This proposed method is believed to reduce the risk of probe

movement due to hanging chords. There is also an increased benefit to sterilization because the catheter can be disposable. The ablation generator contains a transmitting circuit which creates a magnetic field from the LC tank circuit. The catheter has a similar LC circuit which is placed within the flux lines of the transmitting magnetic field. Thus, inducing a voltage across the circuit. The alternating electrical current is then directed through tissues and heat is generated by ionic agitation. During testing, the average maximum received power was 15W where an average maximum efficiency was 63.27% was recorded. The system was able to abate a 2 cm zone when tested with bovine tissue. These results proved that it is possible to perform wireless radiofrequency ablation.

Finally, another wireless ablation system was presented that is similar to the first. In this system, the ablation generator is battery powered. Therefore, the battery powered system is truly wireless during the procedure. Other proposed systems were presented to showcase the future possibilities of this technology. In order to move this technology forward, more research should be conducted to increase the efficiency of the ablation system and improve the design. Further exploration of the field is needed in order to assess the feasibility of using this technology for human medical cases. This technology should go through animal testing and be evaluated to receive an FDA 510(k) clearance approval. In addition to regulation and testing, market research is also needed to examine how and how current physicians use the technology and if they would be willing to adopt a wireless radiofrequency ablation generator.

Table 6.1 gives a simple comparison between the AngioDynamics 1500X RF Generator with single probe catheters and the presented wirelessly powered ablation system [13, 14].

Engineering Specification		Unit	Current Device Value	Target Value	Presented System
Catheter	Ablation Tip Length	cm	1-2.5	1 ± 2	≤ 3
	Probe Diameter	gauge	17	17 ± 3	~6.5, 14
	Thermocouple?	Yes/No	Yes	Yes	No
	Catheter Wired to Generator?	Yes/No	Yes	No	No
Generator	Generator Power	W	1-250	> 2.5	1-15
	Generator Frequency	kHz	460	1-500	50, 220
	Ablation Type	Bi/Mono	Monopolar	Bipolar	Bipolar
	Temperature Control?	Yes/No	Yes	Yes	No
Results	Maximum Ablation Length	cm	2.75	≥ 2.75	2 - 3
	Maximum Ablation Width	cm	1	≥ 1	1 - 2
	Ablation Time	mins	10	any	5
	Temperature at Tip	°C	> 60	> 60	> 60

Table 6.1. Engineering Specifications of Current Device Compared to the Presented System

REFERENCES

- [1] W. C. J. S. e. Brown, "The history of wireless power transmission," vol. 56, no. 1, pp. 3-21, 1996.
- [2] S. Y. R. Hui, W. Zhong, and C. K. J. I. T. o. P. e. Lee, "A critical review of recent progress in mid-range wireless power transfer," vol. 29, no. 9, pp. 4500-4511, 2013.
- [3] L. Xie, Y. Shi, Y. T. Hou, and A. J. I. W. C. Lou, "Wireless power transfer and applications to sensor networks," vol. 20, no. 4, pp. 140-145, 2013.
- [4] C. C. Mi, G. Buja, S. Y. Choi, and C. T. J. I. T. o. I. E. Rim, "Modern advances in wireless power transfer systems for roadway powered electric vehicles," vol. 63, no. 10, pp. 6533-6545, 2016.
- [5] J. Moore, S. Castellanos, S. Xu, B. Wood, H. Ren, and Z. T. H. J. A. o. b. e. Tse, "Applications of Wireless Power Transfer in Medicine: State-of-the-Art Reviews," vol. 47, no. 1, pp. 22-38, 2019.
- [6] S. A. J. A. o. S. O. Curley, "Radiofrequency ablation of malignant liver tumors," vol. 10, no. 4, pp. 338-347, 2003.
- [7] A. N. Mirza *et al.*, "Radiofrequency ablation of solid tumors," vol. 7, no. 2, pp. 95-102, 2001.
- [8] C. L. Brace, "Radiofrequency and microwave ablation of the liver, lung, kidney, and bone: what are the differences?," *Current problems in diagnostic radiology*, vol. 38, no. 3, pp. 135-143, 2009.
- [9] S. N. Goldberg, G. S. Gazelle, L. Solbiati, W. J. Rittman, and P. R. Mueller, "Radiofrequency tissue ablation: increased lesion diameter with a perfusion electrode," *Academic radiology*, vol. 3, no. 8, pp. 636-644, 1996.
- [10] D. E. Haines, "The biophysics of radiofrequency catheter ablation in the heart: the importance of temperature monitoring," *Pacing and Clinical Electrophysiology*, vol. 16, no. 3, pp. 586-591, 1993.
- [11] D. Haemmerich, "Mathematical modeling of impedance controlled radiofrequency tumor ablation and ex-vivo validation," *Conference proceedings : ... Annual International Conference of the IEEE Engineering in Medicine and Biology Society. IEEE Engineering in Medicine and Biology Society. Annual Conference*, vol. 2010, pp. 1605-1608, 2010.
- [12] D. Haemmerich, "Biophysics of radiofrequency ablation," *Critical Reviews™ in Biomedical Engineering*, vol. 38, no. 1, 2010.
- [13] AngioDynamics, "Starburst Radiofrequency Ablation Electrodes," ed, 2016.
- [14] H. Rathke *et al.*, "Comparison of four radiofrequency ablation systems at two target volumes in an ex vivo bovine liver model," *Diagnostic and interventional radiology*, vol. 20, no. 3, p. 251, 2014.
- [15] J. I. Agbinya, *Wireless power transfer*. River Publishers, 2015.

- [16] A. Kurs, A. Karalis, R. Moffatt, J. D. Joannopoulos, P. Fisher, and M. Soljačić, "Wireless power transfer via strongly coupled magnetic resonances," *science*, vol. 317, no. 5834, pp. 83-86, 2007.
- [17] J. R. Reitz, F. J. Milford, and R. W. Christy, *Foundations of electromagnetic theory*. Addison-Wesley Publishing Company, 2008.
- [18] A. Karalis, J. D. Joannopoulos, and M. Soljačić, "Efficient wireless non-radiative mid-range energy transfer," *Annals of Physics*, vol. 323, no. 1, pp. 34-48, 2008.
- [19] J. Baillie, *Gastrointestinal endoscopy: Basic principles and practice*. Butterworth-Heinemann, 1992.
- [20] J.-D. Kim, C. Sun, and I.-S. Suh, "A proposal on wireless power transfer for medical implantable applications based on reviews," in *Wireless Power Transfer Conference (WPTC), 2014 IEEE*, 2014, pp. 166-169: IEEE.
- [21] H. A. T. DIRECTIVE, "Council Directive 90/385/EEC of 20 June 1990 on the approximation of the laws of the Member States relating to active implantable medical devices," *Official Journal L*, vol. 189, no. 20/07, pp. 0017-0036, 1990.
- [22] W. H. Maisel, "Improving the security and privacy of implantable medical devices," *The New England journal of medicine*, vol. 362, no. 13, p. 1164, 2010.
- [23] K. B. Rasmussen, C. Castelluccia, T. S. Heydt-Benjamin, and S. Capkun, "Proximity-based access control for implantable medical devices," in *Proceedings of the 16th ACM conference on Computer and communications security*, 2009, pp. 410-419: ACM.
- [24] B. Surawicz and T. Knilans, *Chou's Electrocardiography in Clinical Practice E-Book: Adult and Pediatric*. Elsevier Health Sciences, 2008.
- [25] P. Berdat, E. Gygax, U. Nydegger, and T. Carrel, "Short-and long-term mechanical cardiac assistance," *The International journal of artificial organs*, vol. 24, no. 5, pp. 263-273, 2001.
- [26] D. Vilkomerson and T. Chilipka, "Implantable Doppler system for self-monitoring vascular grafts," in *Ultrasonics Symposium, 2004 IEEE*, 2004, vol. 1, pp. 461-465: IEEE.
- [27] Google Scholar. Available: <https://scholar.google.com/>
- [28] ScienceDirect. Available: <http://www.sciencedirect.com/>
- [29] IEEE Xplore. Available: <http://ieeexplore.ieee.org/Xplore/home.jsp>
- [30] T. Campi, S. Cruciani, F. Palandrani, V. De Santis, A. Hirata, and M. Feliziani, "Wireless power transfer charging system for AIMDs and pacemakers," *IEEE transactions on microwave theory and techniques*, vol. 64, no. 2, pp. 633-642, 2016.
- [31] J. S. Ho *et al.*, "Wireless power transfer to deep-tissue microimplants," *Proceedings of the National Academy of Sciences*, vol. 111, no. 22, pp. 7974-7979, 2014.
- [32] S. Gabriel, R. Lau, and C. Gabriel, "The dielectric properties of biological tissues: III. Parametric models for the dielectric spectrum of tissues," *Physics in medicine and biology*, vol. 41, no. 11, p. 2271, 1996.
- [33] T. D. Dissanayake *et al.*, "A novel low temperature transcutaneous energy transfer system suitable for high power implantable medical devices: performance and validation in sheep," *Artificial organs*, vol. 34, no. 5, 2010.
- [34] S.-Y. Lee *et al.*, "A programmable implantable microstimulator SoC with wireless telemetry: Application in closed-loop endocardial stimulation for cardiac pacemaker," *IEEE transactions on biomedical circuits and systems*, vol. 5, no. 6, pp. 511-522, 2011.
- [35] P. Li and R. Bashirullah, "A wireless power interface for rechargeable battery operated medical implants," *IEEE Transactions on Circuits and Systems II: Express Briefs*, vol. 54, no. 10, pp. 912-916, 2007.

- [36] G. Monti, M. V. De Paolis, L. Corchia, L. Tarricone, and M. Mongiardo, "Wireless power link for rechargeable pacemakers," in *Advanced Materials and Processes for RF and THz Applications (IMWS-AMP), 2017 IEEE MTT-S International Microwave Workshop Series on*, 2017, pp. 1-3: IEEE.
- [37] C. Kim *et al.*, "Design of miniaturized wireless power receivers for mm-sized implants," in *Custom Integrated Circuits Conference (CICC), 2017 IEEE*, 2017, pp. 1-8: IEEE.
- [38] V. S. Polikov, P. A. Tresco, and W. M. Reichert, "Response of brain tissue to chronically implanted neural electrodes," *Journal of neuroscience methods*, vol. 148, no. 1, pp. 1-18, 2005.
- [39] H. Lee, R. V. Bellamkonda, W. Sun, and M. E. Levenston, "Biomechanical analysis of silicon microelectrode-induced strain in the brain," *Journal of neural engineering*, vol. 2, no. 4, p. 81, 2005.
- [40] G. C. McConnell, H. D. Rees, A. I. Levey, C.-A. Gutekunst, R. E. Gross, and R. V. Bellamkonda, "Implanted neural electrodes cause chronic, local inflammation that is correlated with local neurodegeneration," *Journal of neural engineering*, vol. 6, no. 5, p. 056003, 2009.
- [41] L. Karumbaiah *et al.*, "Relationship between intracortical electrode design and chronic recording function," *Biomaterials*, vol. 34, no. 33, pp. 8061-8074, 2013.
- [42] S. Ha *et al.*, "Silicon-integrated high-density electrocortical interfaces," *Proceedings of the IEEE*, vol. 105, no. 1, pp. 11-33, 2017.
- [43] R. Muller *et al.*, "A minimally invasive 64-channel wireless μ ECoG implant," *IEEE Journal of Solid-State Circuits*, vol. 50, no. 1, pp. 344-359, 2015.
- [44] M. Mark, *Powering mm-size wireless implants for brain-machine interfaces*. University of California, Berkeley, 2011.
- [45] M. Zargham and P. G. Gulak, "Fully Integrated On-Chip Coil in $0.13\ \mu\text{m}$ CMOS for Wireless Power Transfer Through Biological Media," *IEEE transactions on biomedical circuits and systems*, vol. 9, no. 2, pp. 259-271, 2015.
- [46] G. Monti, P. Arcuti, and L. Tarricone, "Resonant inductive link for remote powering of pacemakers," *IEEE Transactions on Microwave Theory and Techniques*, vol. 63, no. 11, pp. 3814-3822, 2015.
- [47] P. Gay-Balmaz and O. J. Martin, "Electromagnetic resonances in individual and coupled split-ring resonators," *Journal of applied physics*, vol. 92, no. 5, pp. 2929-2936, 2002.
- [48] B. H. Waters, A. P. Sample, P. Bonde, and J. R. Smith, "Powering a ventricular assist device (VAD) with the free-range resonant electrical energy delivery (FREE-D) system," *Proceedings of the IEEE*, vol. 100, no. 1, pp. 138-149, 2012.
- [49] A. Cobo, H. Tu, R. Sheybani, and E. Meng, "Characterization of a wireless implantable infusion micropump for small animal research under simulated in vivo conditions," in *Biomedical Circuits and Systems Conference (BioCAS), 2014 IEEE*, 2014, pp. 348-351: IEEE.
- [50] S. C. Tang, T. L. T. Lun, Z. Guo, K.-W. Kwok, and N. J. McDannold, "Intermediate range wireless power transfer with segmented coil transmitters for implantable heart pumps," *IEEE Transactions on Power Electronics*, vol. 32, no. 5, pp. 3844-3857, 2017.
- [51] R. Puers, R. Carta, and J. Thoné, "Wireless power and data transmission strategies for next-generation capsule endoscopes," *Journal of Micromechanics and Microengineering*, vol. 21, no. 5, p. 054008, 2011.

- [52] W. Xin, G. Yan, and W. Wang, "Study of a wireless power transmission system for an active capsule endoscope," *The international journal of medical robotics and computer assisted surgery*, vol. 6, no. 1, pp. 113-122, 2010.
- [53] S. C. Tang, F. A. Jolesz, and G. T. Clement, "A wireless batteryless deep-seated implantable ultrasonic pulser-receiver powered by magnetic coupling," *IEEE transactions on ultrasonics, ferroelectrics, and frequency control*, vol. 58, no. 6, 2011.
- [54] S. C. Tang, "A low-operating-voltage wireless intermediate-range scheme for energy and signal transmission by magnetic coupling for implantable devices," *IEEE Journal of Emerging and Selected Topics in Power Electronics*, vol. 3, no. 1, pp. 242-251, 2015.
- [55] S. C. Tang, D. Vilkomerson, and T. Chilipka, "Magnetically-powered implantable Doppler blood flow meter," in *Ultrasonics Symposium (IUS), 2014 IEEE International*, 2014, pp. 1622-1625: IEEE.
- [56] L. Kim, S. C. Tang, and S.-S. Yoo, "Prototype modular capsule robots for capsule endoscopies," in *Control, Automation and Systems (ICCAS), 2013 13th International Conference on*, 2013, pp. 350-354: IEEE.
- [57] H. Vihvelin, J. Leadbetter, M. Bance, J. A. Brown, and R. B. Adamson, "Class E RF amplifier design in an ultrasonic link for wireless power delivery to implanted medical devices," in *Electrical and Computer Engineering (CCECE), 2015 IEEE 28th Canadian Conference on*, 2015, pp. 382-386: IEEE.
- [58] K. J. Parker, R. M. Lerner, and R. C. Waag, "Attenuation of ultrasound: magnitude and frequency dependence for tissue characterization," *Radiology*, vol. 153, no. 3, pp. 785-788, 1984.
- [59] X. Liu, F. Zhang, S. A. Hackworth, R. J. Scwabassi, and M. Sun, "Wireless power transfer system design for implanted and worn devices," in *Bioengineering Conference, 2009 IEEE 35th Annual Northeast*, 2009, pp. 1-2: IEEE.
- [60] B. Lenaerts and R. Puers, "An inductive power link for a wireless endoscope," *Biosensors and Bioelectronics*, vol. 22, no. 7, pp. 1390-1395, 2007.
- [61] L. Feng, Y. Mao, and Y. Cheng, "An efficient and stable power management circuit with high output energy for wireless powering capsule endoscopy," in *Solid State Circuits Conference (A-SSCC), 2011 IEEE Asian*, 2011, pp. 229-232: IEEE.
- [62] T. Sun, X. Xie, G. Li, Y. Gu, Y. Deng, and Z. Wang, "A two-hop wireless power transfer system with an efficiency-enhanced power receiver for motion-free capsule endoscopy inspection," *IEEE transactions on Biomedical Engineering*, vol. 59, no. 11, pp. 3247-3254, 2012.
- [63] X. Fang, H. Liu, G. Li, Q. Shao, and H. Li, "Wireless power transfer system for capsule endoscopy based on strongly coupled magnetic resonance theory," in *Mechatronics and Automation (ICMA), 2011 International Conference on*, 2011, pp. 232-236: IEEE.
- [64] K. Shiba, A. Morimasa, and H. Hirano, "Design and development of low-loss transformer for powering small implantable medical devices," *IEEE transactions on biomedical circuits and systems*, vol. 4, no. 2, pp. 77-85, 2010.
- [65] S. B. Lee, H.-M. Lee, M. Kiani, U.-M. Jow, and M. Ghovanloo, "An inductively powered scalable 32-channel wireless neural recording system-on-a-chip for neuroscience applications," *IEEE transactions on biomedical circuits and systems*, vol. 4, no. 6, pp. 360-371, 2010.

- [66] S. O'Driscoll, A. S. Poon, and T. H. Meng, "A mm-sized implantable power receiver with adaptive link compensation," in *Solid-State Circuits Conference-Digest of Technical Papers, 2009. ISSCC 2009. IEEE International*, 2009, pp. 294-295, 295 a: IEEE.
- [67] J. Yoo, L. Yan, S. Lee, Y. Kim, and H.-J. Yoo, "A 5.2 mW Self-Configured Wearable Body Sensor Network Controller and a 12 μ W Wirelessly Powered Sensor for a Continuous Health Monitoring System," *IEEE Journal of Solid-State Circuits*, vol. 45, no. 1, pp. 178-188, 2010.
- [68] H. Nakamoto *et al.*, "A passive UHF RFID tag LSI with 36.6% efficiency CMOS-only rectifier and current-mode demodulator in 0.35 μ m FeRAM technology," in *Solid-State Circuits Conference, 2006. ISSCC 2006. Digest of Technical Papers. IEEE International*, 2006, pp. 1201-1210: IEEE.
- [69] M. Ghovanloo and K. Najafi, "Fully integrated wideband high-current rectifiers for inductively powered devices," *IEEE Journal of Solid-State Circuits*, vol. 39, no. 11, pp. 1976-1984, 2004.
- [70] A. Kornbluth, J. Colombel, J. A. Leighton, and E. Loftus, "ICCE consensus for inflammatory bowel disease," *Endoscopy*, vol. 37, no. 10, pp. 1051-1054, 2005.
- [71] P. Swain, "Wireless capsule endoscopy," *Gut*, vol. 52, no. suppl 4, pp. iv48-iv50, 2003.
- [72] R. de Franchis, A. Avgerinos, J. Barkin, D. Cave, and B. Filoche, "ICCE consensus for bowel preparation and prokinetics," *Endoscopy*, vol. 37, no. 10, pp. 1040-1045, 2005.
- [73] I. Fuyuno, "Olympus finds market rival hard to swallow," *Nature*, vol. 438, no. 7070, pp. 913-913, 2005.
- [74] I. C. o. N.-I. R. Protection, "ICNIRP statement on the "guidelines for limiting exposure to time-varying electric, magnetic, and electromagnetic fields (up to 300 ghz)," *Health physics*, vol. 97, no. 3, pp. 257-258, 2009.
- [75] U. CEPT, "Electromagnetic compatibility and Radio spectrum Matters (ERM); Radio Frequency Identification Equipment operating in the band 865 MHz to 868 MHz with power levels up to 2 W; Part 1: Technical requirements and methods of measurement [Internet]," ed: Internet, 2005.
- [76] (2018). *Grantome*. Available: <http://grantome.com/search?q=Bradford+Wood>
- [77] G. S. Gazelle, S. N. Goldberg, L. Solbiati, and T. Livraghi, "Tumor ablation with radio-frequency energy," *Radiology*, vol. 217, no. 3, pp. 633-646, 2000.
- [78] P. F. Laeseke *et al.*, "Multiple-electrode radiofrequency ablation creates confluent areas of necrosis: in vivo porcine liver results," *Radiology*, vol. 241, no. 1, pp. 116-124, 2006.
- [79] Z. Liu, M. Ahmed, Y. Weinstein, M. Yi, R. L. Mahajan, and S. N. Goldberg, "Characterization of the RF ablation-induced 'oven effect': The importance of background tissue thermal conductivity on tissue heating," *International Journal of Hyperthermia*, vol. 22, no. 4, pp. 327-342, 2006/01/01 2006.
- [80] J. H. Baek, J. H. Lee, R. Valcavi, C. M. Pacella, H. Rhim, and D. G. Na, "Thermal ablation for benign thyroid nodules: radiofrequency and laser," *Korean Journal of Radiology*, vol. 12, no. 5, pp. 525-540, 2011.
- [81] S. M. Lobo, K. S. Afzal, M. Ahmed, J. B. Kruskal, R. E. Lenkinski, and S. N. Goldberg, "Radiofrequency ablation: modeling the enhanced temperature response to adjuvant NaCl pretreatment," *Radiology*, vol. 230, no. 1, pp. 175-182, 2004.
- [82] M. Inc., "Cool-tip RF Ablation System E Series," ed, 2017.
- [83] NeuWave, "NeuWave Microwave Ablation System," 2017.
- [84] G. O. Phillips and P. A. Williams, *Handbook of Hydrocolloids*. CRC Press, 2000.

- [85] D. M. Otten and B. Rubinsky, "Cryosurgical monitoring using bioimpedance measurements—a feasibility study for electrical impedance tomography," *IEEE Transactions on Biomedical Engineering*, vol. 47, no. 10, pp. 1376-1381, 2000.
- [86] G. Qiao, W. Wang, L. Wang, Y. He, B. Bramer, and M. Al-Akaidi, "Investigation of biological phantom for 2D and 3D breast EIT images," Berlin, Heidelberg, 2007, pp. 328-331: Springer Berlin Heidelberg.
- [87] A. S. Mikhail, A. H. Negussie, C. Graham, M. Mathew, B. J. Wood, and A. Partanen, "Evaluation of a tissue-mimicking thermochromic phantom for radiofrequency ablation," *Medical physics*, vol. 43, no. 7, pp. 4304-4304, 2016.
- [88] S. J. Medical, "Ablation Therapy Device Compatibility Matrix," ed. St. Paul, MN: Abbott, 2017.
- [89] Covidien, "Owners Manual," C. R. Generator, Ed., ed. Medtronic, 2014.
- [90] S. A. Solazzo *et al.*, "Radiofrequency ablation: importance of background tissue electrical conductivity—an agar phantom and computer modeling study," *Radiology*, vol. 236, no. 2, pp. 495-502, 2005.
- [91] T. Morimoto *et al.*, "A Study of the Electrical Bio-impedance of Tumors," *Journal of Investigative Surgery*, vol. 6, no. 1, pp. 25-32, 1993/01/01 1993.
- [92] H. Iida, T. Aihara, S. Ikuta, and N. Yamanaka, "Effectiveness of impedance monitoring during radiofrequency ablation for predicting popping," *World journal of gastroenterology*, vol. 18, no. 41, pp. 5870-5878, 2012.
- [93] E. M. Knavel and C. L. Brace, "Tumor ablation: common modalities and general practices," *Techniques in vascular and interventional radiology*, vol. 16, no. 4, pp. 192-200, 2013.
- [94] E. Blessing, M. D. Esler, D. P. Francis, and R. E. J. J. C. I. Schmieder, "Cardiac ablation and renal denervation systems have distinct purposes and different technical requirements," vol. 6, no. 3, p. 314, 2013.
- [95] Y.-C. Joo, J.-Y. Park, and K.-H. J. J. o. a. Kim, "Comparison of alcohol ablation with repeated thermal radiofrequency ablation in medial branch neurotomy for the treatment of recurrent thoracolumbar facet joint pain," vol. 27, no. 3, pp. 390-395, 2013.
- [96] N. Patel, A. Gross, L. Brown, and G. J. P. M. Gekht, "A randomized, placebo-controlled study to assess the efficacy of lateral branch neurotomy for chronic sacroiliac joint pain," vol. 13, no. 3, pp. 383-398, 2012.
- [97] T. Livraghi, S. N. Goldberg, S. Lazzaroni, F. Meloni, L. Solbiati, and G. S. J. R. Gazelle, "Small hepatocellular carcinoma: treatment with radio-frequency ablation versus ethanol injection," vol. 210, no. 3, pp. 655-661, 1999.
- [98] A. S. Pearson *et al.*, "Intraoperative radiofrequency ablation or cryoablation for hepatic malignancies," vol. 178, no. 6, pp. 592-598, 1999.
- [99] R. Souchon *et al.*, "Visualisation of HIFU lesions using elastography of the human prostate in vivo: preliminary results," vol. 29, no. 7, pp. 1007-1015, 2003.
- [100] A. Vogel and V. J. C. r. Venugopalan, "Mechanisms of pulsed laser ablation of biological tissues," vol. 103, no. 2, pp. 577-644, 2003.
- [101] S. Y. Nakada *et al.*, "Bipolar radiofrequency ablation of the kidney: comparison with monopolar radiofrequency ablation," vol. 17, no. 10, pp. 927-933, 2003.
- [102] B. Decadt and A. K. J. T. I. o. Siriwardena, "Radiofrequency ablation of liver tumours: systematic review," vol. 5, no. 9, pp. 550-560, 2004.

- [103] J. P. McGahan and G. D. J. A. J. o. R. Dodd III, "Radiofrequency ablation of the liver: current status," vol. 176, no. 1, pp. 3-16, 2001.
- [104] J. Machi *et al.*, "Ultrasound-guided radiofrequency thermal ablation of liver tumors: percutaneous, laparoscopic, and open surgical approaches," vol. 5, no. 5, pp. 477-489, 2001.
- [105] M. P. S. Boeti, R. z. Grigorie, and I. Popescu, "Laparoscopic radiofrequency ablation of liver tumors," in *Hepatic Surgery*: IntechOpen, 2013.
- [106] K. Y. Kim, *Wireless power transfer-principles and engineering explorations*. 2012.
- [107] O. H. Stielau and G. A. Covic, "Design of loosely coupled inductive power transfer systems," in *PowerCon 2000. 2000 International Conference on Power System Technology. Proceedings (Cat. No. 00EX409)*, 2000, vol. 1, pp. 85-90: IEEE.
- [108] B. T. William, *Advanced Electromagnetism: Foundations: Theory And Applications*. World Scientific, 1995.
- [109] A. Costanzo, M. Dionigi, F. Mastri, and M. Mongiardo, "Rigorous modeling of mid-range wireless power transfer systems based on Royer oscillators," in *2013 IEEE Wireless Power Transfer (WPT)*, 2013, pp. 69-72: IEEE.
- [110] F. Mastri, A. Costanzo, M. Dionigi, and M. Mongiardo, "Harmonic balance design of wireless resonant-type power transfer links," in *2012 IEEE MTT-S International Microwave Workshop Series on Innovative Wireless Power Transmission: Technologies, Systems, and Applications*, 2012, pp. 245-248: IEEE.
- [111] P. Kovoov *et al.*, "Effect of Inter-electrode Distance on Bipolar Intramural Radiofrequency Ablation," vol. 28, no. 6, pp. 514-520, 2005.